Tesi doctoral presentada per En/Na

Marc MANERA MIRET

amb el títol

"Cosmologia i Formació d'Estructures"

per a l'obtenció del títol de Doctor/a en

CIÈNCIES FÍSIQUES

Barcelona, 27 de juny del 2007.

Facultat de Física
Departament de Física Fonamental

UNIVERSITAT DE BARCELONA

Part I

Growth of Struture in Non-Standard Cosmologies

Chapter 2

The Emergence of a new cosmological paradigm

Summary

In this chapter I introduce the new cosmological paradigm and the perturbation theory for the standard ΛCDM cosmology. I also comment on the possibility of explaining the accelerated expansion of the universe with non-standard models.

2.1 A late time accelerated universe

In the last decade there has been an increasing and compelling evidence for a change in a cosmological paradigm. Observations of type Ia supernovae (Perlmutter et al. 1999) as well as the Cosmic Microwave Background (CMB) radiation (Spergel et al. 2003) and large scale structure of the universe (Efstathiou et al. 1990; Zehavi et al. 2002) have pointed consistently towards a new cosmological paradigm: a nearly flat universe that is currently undertaking a phase of accelerated expansion.

This accelerated expansion can not be explained by an Einstein-de-Sitter universe, where the matter density is equal to the critical one, nor it can be reconciled with an open universe with much less dark matter. A more substantial change in the cosmological model is needed, being the

introduction of a cosmological constant in the Einstein equations the most simple of the proposed solutions to match observations. This is the so called ΛCDM model.

There are possibly only two main theoretical approaches to embrace the observational evidence of a currently accelerated expansion of the universe. The first one is changing our understanding of gravity, which actually translates in a modification of the right hand side of the Einstein equations. This is, for instance, the approach of the Dvli Gabadadze Porrati model (Dvali et al. 2000) or the $f(R)$ cosmologies (Nojiri 2006). The second option is to modify the left hand side of the Einstein equations by introducing a new component in the energy-momentum tensor. This new component is called dark energy. It is to be understood as an energy that fills the universe, which, in order to contribute to accelerate the universe, has an anomalous equation of state with $p < -\frac{1}{3}\rho$. The most popular dark energy candidates are the vacuum energy and the scalar fields, also known as quientessence (Ratra and Peebles 1988; Wetterich 2001). The term dark energy, however, is sometimes used in a broader sense (not that of this thesis), i.e., whatever it makes the universe to accelerate.

It is easy to see that by moving terms from one side of the Einstein's equations to the other we can recall non-standard gravitational theories as being effective dark energy models with general equation of state $p = w(z)\rho$. The particular case of $w = -1$, whether it comes from a cosmological constant or from a vacuum dark energy, or both, corresponds to the new cosmological paradigm, the ΛCDM model, which will be explained in section 2.2 below.

Apart from the two theoretical options mentioned before, there is still a third one,which would not require to modify Einstein equations. It is to consider backreaction from dark matter fluctuations as a possible source for cosmological expansion. (Rasanen 2004; Martineau and Brandenberger 2005). This is a very controversial approach and seems not to successfully reproduce supernovae observations so far.

In the chapters 4 5 6 and 7 we will look at different models of both dark energy and modification of gravity approaches in order to see if there are cosmological signatures that could allow us to differentiate them to the new concordance model.

2.2 The ΛCDM cosmology

At very big scales the universe is seen as highly homogeneous and isotropic and can be well described by the Friedmann-Robertson-Walker metric:

$$ds^2 = dt^2 - a(t)^2(dx^2/(1-kx^2 + x^2(d\theta + sin(\theta)^2 d\phi^2)) \tag{2.1}$$

where we set $c = 1$ and a is the scale factor. We have $k = 0, 1, -1$ for a flat, closed or open universe respectively. The dynamics of the universe will be given by the Einstein's equations:

$$G_{\mu\nu} \equiv R_{\mu\nu} - \frac{1}{2} g_{\mu\nu} R - \Lambda g_{\mu\nu} = -8\pi G T_{\mu\nu} \tag{2.2}$$

The assumption of homogeneity and isotropy implies that $T_{\mu\nu}$ has a diagonal form, which when considering an ideal fluid is $T^{\mu}_{\nu} = dia[\rho(t), -p(t), -p(t), -p(t)]$. In this case, the only two non-trivial and independent Einstein's equations are:

$$\frac{\dot{a}^2}{a^2} + \frac{k}{a^2} = \frac{8\pi G \rho(t)}{3} + \frac{\Lambda}{3} \tag{2.3}$$

$$\frac{2\ddot{a}}{a} + \frac{\dot{a}^2}{a^2} + \frac{k}{a^2} = -8\pi G p(t) + \Lambda \tag{2.4}$$

Either from $T_{\mu\nu;\nu}$ or equivalently by deriving equation 2.3 and using 2.4 to get rid of $\ddot{a}$ one and obtain the continuity equation

$$\dot{\rho} + 3H(\rho + p) = 0 \tag{2.5}$$

Where $H \equiv \dot{a}/a$. When having $p = p(\rho)$ the continuity equation gives the evolution of the density with the scale factor. For the general form $p = w(a)\rho$ it results in $\rho = \rho_0 \exp \int -3(1+w)\frac{da}{a}$. Obviously for non relativistic matter ($p = 0$) and for radiation ($p = 1/3\rho$) we recover $\rho_m = \rho_m(0)/a^3$ and $\rho_r = \rho_r(0)/a^4$ respectively. The cosmological constant can be also understood as a constant dark energy density with implies $p = -\rho$. The equation 2.3 is called Friedman equation and can be rewritten as

$$H^2 = \left(\frac{\dot{a}}{a}\right)^2 = H_0^2 \left(\frac{\Omega_m}{a^3} + \frac{\Omega_r}{a^4} + \frac{\Omega_k}{a^2} + \Omega_\Lambda\right) \tag{2.6}$$

where we have introduced the Ω's cosmological parameters. They can be expressed as a function of the critical density $\rho_c = \frac{3H_0^2}{8\pi G}$: $\Omega_m = \frac{8\pi G}{3H_0^2}\rho_{m,0} = \frac{\rho_{m,0}}{\rho_c}$, $\Omega_r = \frac{8\pi G}{3H_0^2}\rho_{r,0} = \frac{\rho_{r,0}}{\rho_c}$, $\Omega_\Lambda = \frac{\Lambda}{3H_0^2}$,$\Omega_k = \frac{-k}{H_0^2}$ and by definition they hold the $\Omega_m + \Omega_r + \Omega_\Lambda + \Omega_k = 1$ normalization. The subindex 0 in any variable will always mean to get its current $z = 0$ value.

By introducing equation 2.3 into equation 2.4 one gets

$$\dot{H} + H^2 = \frac{\ddot{a}}{a} = -\frac{4\pi G}{3}(\rho + 3p) + \frac{\Lambda}{3} \tag{2.7}$$

Notice that equation 2.7 is derived from Einstein's equations. We could also arrive to it by using Friedman equation 2.6 and the continuity equation 2.5. This will be important for non-standard cosmological models where gravity is changed, as we will explain in chapter 3.

The Concordance Model

We use the term Concordance Model for the ΛCDM model once we have fixed the Ω's parameters as well as other cosmological parameters to the observed values. The values we use in this thesis as a Concordance Model are $\Omega_m \simeq 0.25 - 0.3$, $\Omega_\Lambda \simeq O.7 - 0.75$, $\Omega_b \simeq 0.045$, $\Omega_r < 0.001 \simeq 0$, $h = H_0/100 \simeq 0.7 - 0.72$, $\sigma_8 \simeq 0.8 - 0.9$,$w = -1$.

2.3 The growth of structure in ΛCDM model

Newtonian Approximation

We can study the evolution of dark matter fluctuations in terms of three quantities: the dark matter density $\rho(\vec{r}, t)$, its velocity field $v(\vec{r}, t)$ and the Newtonian Gravitational Potential Φ, while neglecting at large scales the stress tensor that describes deviations from a coherent flow. The proper justification for a Newtonian treatment can be given only by the appropriate limit from general relativistic equations. For the cold dark matter growth of structure we will assume non-relativistic velocities and consider scales smaller that the Hubble radius. We can start with the standard equations for an ideal fluid: the continuity equation expressing mass conservation and the

Euler equation expressing momentum conservation (see Peebles 1980).

$$\begin{aligned} \frac{\partial \rho}{\partial t} + \nabla_r \cdot \rho \vec{u} = 0 \\ \rho \left[\frac{\partial \vec{u}}{\partial t} + (\vec{u} \cdot \nabla_r)\vec{u} \right] = -\nabla_r p - \rho \nabla_r \Phi \end{aligned} \tag{2.8}$$

The velocity field is the Hubble flow plus a contribution from the peculiar physical velocity

$$\vec{u} = \frac{d}{dt}(a\vec{x}) = \dot{a}\vec{x} + a\dot{\vec{x}} = H\vec{r} + \vec{v} \tag{2.9}$$

It will be more convenient to express the fluid equations in expanding coordinates $(t, \vec{x})$. With this change we get

$$\begin{aligned} \frac{\partial \delta}{\partial t} + 3\frac{\dot{a}}{a}\rho + \frac{1}{a}\nabla \cdot \rho \vec{v} = 0 \\ \frac{\partial \vec{v}}{\partial t} + \frac{1}{a}(\vec{v} \cdot \nabla)\vec{v} + \frac{\dot{a}}{a}\vec{v} = -\frac{1}{\rho a}\nabla p - \frac{1}{a}\nabla \phi \end{aligned} \tag{2.10}$$

Here, ϕ is the potential for the perturbed density, which follows the Poisson equation

$$\nabla^2 \phi = 4\pi G a^2 (\rho(t, \vec{x}) - \bar{\rho}) \tag{2.11}$$

where $\bar{\rho}$ is the comoving background matter density. In order to arrive to an equation for the evolution of density fluctuations we take the divergence of the second equation 2.10. We can express it in terms of the shear σ the vorticity ω and $\theta = \nabla \cdot \vec{v}$. And by making use of the following decomposition

$$\frac{v^{\alpha}_{,\beta}}{a} = \frac{1}{3}\frac{\theta}{a}\delta^{\alpha\beta} + \sigma_{\alpha\beta} - \omega_{\alpha\beta} \tag{2.12}$$

we arrive to

$$\left(\frac{\partial}{\partial t} + 2\frac{\dot{a}}{a} + \frac{1}{a}\vec{v} \cdot \nabla \right) \frac{\theta}{a} + \frac{\theta^2}{3a^2} + \sigma^2 - \omega^2 = -4\pi G(\rho - \bar{\rho}) - \frac{\nabla^2 p}{\rho a^2} \tag{2.13}$$

The Relativistic Raychaudhuri's equation in the Spherical Collapse

In General Relativity the gravitational growth of structures can be studied starting with the Raychaudhuri's equation (Raychaudhuri 1955). The interest in this equation comes from the fact that one can study the convergence of a congruence of geodesics from it. The Raychaudhuri's equation has the special characteristic that it is true without reference to Einstein's equations, thus being very useful for studying non standard cosmologies. For a shear-free fluid with no vorticity and a four-velocity u^μ the Raychaudhuri's equation is,

$$\dot{\Theta} + \frac{1}{3}\Theta^2 = R_{\mu\nu}u^\mu u^\nu \tag{2.14}$$

where $\Theta \equiv \nabla_\mu u^\mu$. Again, choosing the coordinate system such that the four-velocity of the fluid, u^μ, is expressed as the Hubble flow plus the peculiar velocity $\mathbf{v}$, $u^\mu = (1, \dot{a}\mathbf{x} + \mathbf{v})$, we get

$$\Theta = 3\frac{\dot{a}}{a} + \frac{\theta}{a}, \tag{2.15}$$

where we have defined $\theta \equiv \nabla \cdot \mathbf{v}$. Thus we can rewrite the Raychaudhuri's equation as

$$\frac{\dot{\theta}}{a} + \frac{\theta}{a}\bar{H} + \frac{1}{3}\frac{\theta^2}{a^2} = R_{\mu\nu}u^\mu u^\nu - 3(\dot{\bar{H}} + \bar{H}^2). \tag{2.16}$$

Here H is the local perturbed Hubble parameter. The unperturbed (background) Hubble parameter is $\bar{H}$. The $R_{\mu\nu}u^\mu u^\nu$ term is also a local perturbed quantity, and we want to express it in terms of the perturbed density. In the spherical collapse model, we can still use the FRW metric with a slight different source for the Ω's contribution. Thus we get $R_{\mu\nu}u^\mu u^\nu = 3(\dot{H} + H^2)$. By using equation we 2.7 we arrive to the Raychaudhuri's equation for the ΛCDM model. For the case of negligible pressure (like dark matter) we get.

$$\frac{\dot{\theta}}{a} + \frac{\theta}{a}\bar{H} + \frac{1}{3}\frac{\theta^2}{a^2} = -4\pi G(\rho - \bar{\rho}) \tag{2.17}$$

This equation is the same as equation 2.13 with no pressure, shear or vorticity.

The Spherical Collapse Model

In a matter dominated universe, the continuity equation for a non-relativistic ($\rho \gg p$) fluid can be written as ((Peebles 1993))

$$\frac{d\delta}{d\tau} + (1+\delta)\theta = 0, \tag{2.18}$$

where the local density contrast is defined as

$$\delta(\tau, \mathbf{x}) = \frac{\rho(\tau, \mathbf{x})}{\bar{\rho}(\tau)} - 1 \tag{2.19}$$

and we have switched to conformal time $dt = ad\tau$. Using (2.18), (2.19) and (2.17) we see that in terms of the conformal time we get:

$$\frac{d^2\delta}{d\tau^2} + \mathcal{H}\frac{d\delta}{d\tau} - \frac{4}{3}\frac{1}{1+\delta}\left(\frac{d\delta}{d\tau}\right)^2 = 4\pi G\,(1+\delta)\delta\bar{\rho}a^2, \tag{2.20}$$

where $\mathcal{H} \equiv d\,ln(a)/d\tau$. Rescaling the time variable once more, $\eta = \ln(a)$, we arrive at

$$\frac{d^2\delta}{d\eta^2} + (2 + \frac{\dot{\bar{H}}}{\bar{H}^2})\frac{d\delta}{d\eta} - \frac{4}{3}\frac{1}{1+\delta}(\frac{d\delta}{d\tau})^2 = 4\pi G\,(1+\delta)\delta\frac{\bar{\rho}}{\bar{H}^2}. \tag{2.21}$$

Using the notations (2.6), and recalling that in the matter dominated regime it follows from the continuity equation, (2.5), that $\rho \sim a^{-3}$, the Friedmann equation for a flat ΛCDM model can be written as

$$H^2 = H_0^2[\frac{\Omega_M}{a^3} + \Omega_\Lambda]. \tag{2.22}$$

Using this in Eq. (2.21) gives us the well known result of standard perturbation theory.

$$\frac{d^2\delta}{d\eta^2} + \Big[2 - \frac{3}{2}\frac{\Omega_M}{\Omega_M + a^3\Omega_\Lambda}\Big]\frac{d\delta}{d\eta} - \frac{4}{3}\frac{1}{1+\delta}\Big(\frac{d\delta}{d\tau}\Big)^2 = \frac{3}{2}(1+\delta)\delta\frac{\Omega_M}{\Omega_M + a^3\Omega_\Lambda}. \tag{2.23}$$

This is the exact (non-perturbative) spherical collapse equation for the density contrast. It gives the correct result in the linear case as well as in the nonlinear case when considering fluctuations whithin a spherical window. In the Einstein-de-Sitter universe equation 2.23 admits a well known parametric solution (Cooray & Sheth 2002; Gaztanaga & Lobo 2001)

$$\delta(\varphi) = \frac{9}{2}\frac{(\varphi-\sin\varphi)^2}{(1-\cos\varphi)^3} - 1 \tag{2.24}$$

$$\delta_l(\varphi) = \frac{3}{5}\left[\frac{3}{4}(\varphi-\sin\varphi)\right]^{2/3} \tag{2.25}$$

for $\delta_l > 0$, linear overdensity, and

$$\delta(\varphi) = \frac{9}{2}\frac{(\varphi-\sinh\varphi)^2}{(1-\cos\varphi)^3} - 1 \tag{2.26}$$

$$\delta_l(\varphi) = -\frac{3}{5}\left[\frac{3}{4}(\sinh\varphi-\varphi)\right]^{2/3} \tag{2.27}$$

for $\delta_l < 0$, linear under-density (see Peebles 1993). Here the parameter φ is just a parameterization of the time coordinate. For a solution with $\Omega_M \neq 1$ see Bernardeau (1992) and Fosalba & Gaztanaga (1998). Note the singularity at $\delta_l \simeq 1.686$, which corresponds to the gravitational collapse $\delta \to \infty$. The linear density for which structures collapse is called critical density δ_c and its value is weackly dependent on Ω_Λ (Eke et al. 1998).

Solutions for linear and nonlinear growth in Λ CDM

In order to determine how a small perturbation grows with time at different orders in perturbation theory, we expand δ as:

$$\delta = \sum_{i=1}^{\infty}\delta_i = \sum_{i=1}^{\infty}\frac{D_i(\eta)}{i!}\delta_0^i, \tag{2.28}$$

where δ_0 is the small perturbation (and the expansion parameter). Using the expansion, we get the linear equation

$$D_1'' + (2 - \frac{3}{2}\frac{\Omega_M}{\Omega_M + a^3\Omega_\Lambda})D_1' - \frac{3}{2}\frac{\Omega_M}{\Omega_M + a^3\Omega_\Lambda}D_1 = 0, \tag{2.29}$$

which in an Einstein-de-Sitter (EdS) universe ($\Omega_M = 1,\ \Omega_\Lambda = 0$) has the well known solution

$$D_1(\eta) = c_1 e^{\eta} + c_2 e^{-3\eta/2}. \tag{2.30}$$

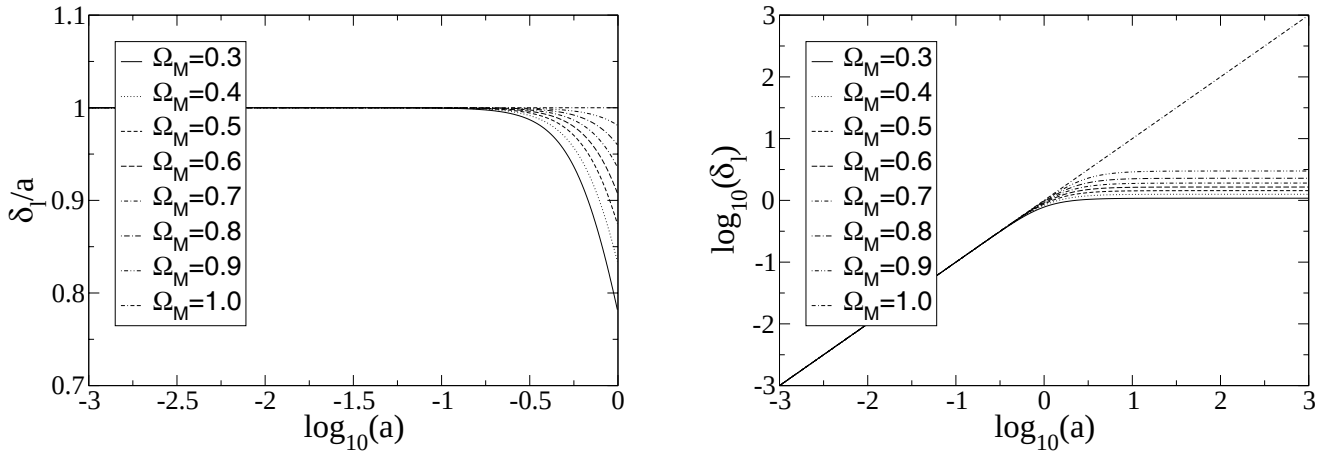

Figure 2.1: Linear growth in the Λ CDM model for different values of Ω_M and $\Omega_M + \Omega_\Lambda = 1$

The solution to the linear equation in the general case with non-zero Λ, can be expressed as (Lahav & Yasushi 2004)

$$D_1 = c_1\, H + c_2\, H \int \frac{da}{a^3 H^3} \tag{2.31}$$

or equivalently, in terms of the hyper-geometric function, as

$$D_1 = \tilde{c}_1 \frac{\sqrt{1 + \frac{\Omega_\Lambda}{\Omega_M} a^3}}{a^{3/2}} + \tilde{c}_2\, {}_2F_1\Big[1, \frac{1}{3}, \frac{11}{6}, -\frac{\Omega_\Lambda}{\Omega_M} a^3\Big] a. \tag{2.32}$$

The second order equation is

$$D_2'' + (2 - \frac{3}{2}\frac{\Omega_M}{\Omega_M + a^3\Omega_\Lambda}) D_2' - \frac{3}{2}\frac{\Omega_M}{\Omega_M + a^3\Omega_\Lambda} D_2 - \frac{8}{3}(D_1')^2 - 3D_1^2 \frac{\Omega_M}{\Omega_M + a^3\Omega_\Lambda} = 0, \tag{2.33}$$

where it is understood that the linear solution is substituted. Similarly one can recursively go on to arbitrary order.

The second order equation determines how Gaussian initial conditions develop non-Gaussian features and can be related to the skewness of the density field at large scale. The q-order moments of the fluctuating field are related to the perturbations by (Bernardeau et. al. 2002)

$$m_q \equiv < \delta^q >, \tag{2.34}$$

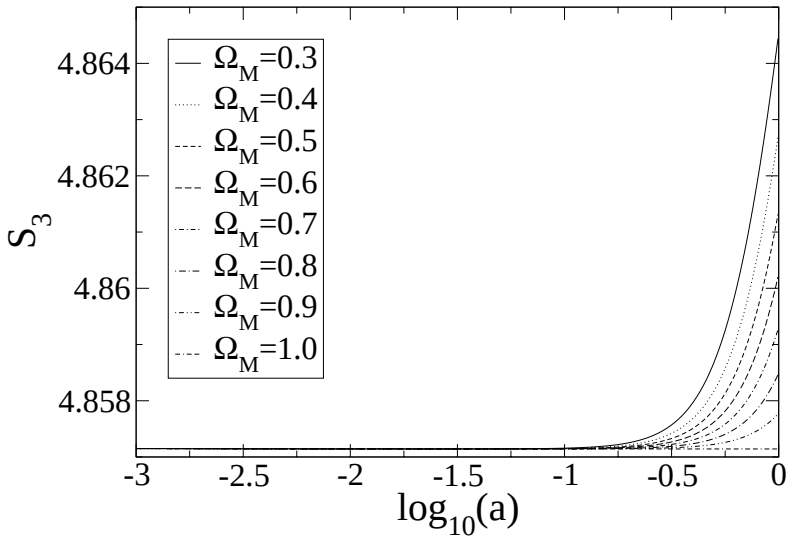

Figure 2.2: Non-linear growth in the Λ CDM model for different values of Ω_M and $\Omega_M + \Omega_\Lambda = 1$

which in term can be related to the connected moments, or cumulants, $\bar{\xi}_q$. The normalized skewness is given by (Bernardeau et. al. 2002)

$$S_3 = \frac{\bar{\xi}_3}{\bar{\xi}_2^2} = \frac{m_3}{m_2^2}, \tag{2.35}$$

which can be written in terms of the first and second order perturbations. For example at leading order:

$$m_3 = \langle \delta^3 \rangle \simeq \langle \delta_1^3 \rangle + 3\langle \delta_2 \ \delta_1^2 \rangle + \dots \tag{2.36}$$

For Gaussian perturbations $\langle \delta_1^3 \rangle = 0$, so that we get:

$$S_3 = \frac{3}{2}\frac{D_2}{D_1^2}. \tag{2.37}$$

In an Einstein-de-Sitter universe this coefficient can be calculated exactly and it is $S_3^{EdS} = 34/7 \approx 4.86$.

To illustrate the effect of the cosmological constant, we have solved the linear and second order equations numerically. The linear evolution and the evolution of S_3 are shown in Fig 2.1 and Fig 2.3.

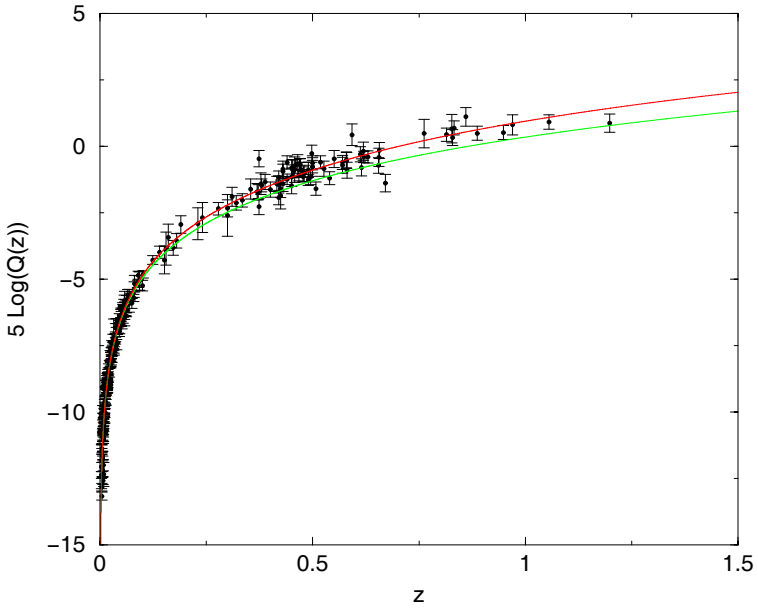

Figure 2.3: Hubble-constant-free luminosity distances from supernova observational data of Tonry et al. (2003) and Barris et al. (2004). The green and red line are the Einstein de Sitter and the concordance ΛCDM ($\Omega_\Lambda = 0.3$) model predictions. It can be seen that the former model does not fit the data

We see that the effect on the linear growth factor is significant as perturbations grow less when the cosmological constant is large compared to the energy density of matter. The effect of the cosmological constant on linear growth is well represented by the other figure where future evolution is shown. With a non-zero Ω_Λ, δ_l freezes and structures stop growing in the future. The effect on S_3 is very small, as expected, so that even when $\Omega_M = 0.3$, $\Delta S_3 < 1\%$. Such a small change is clearly out of reach of present day observations.

2.4 Supernovae observational support for the Concordance Model

Studies of nearby type Ia supernovae have revealed a relationship between the maximum magnitude of the supernova explosion and the width of the lightcurve. The more luminous the supernova is the more days it takes the flux to decrease to the 10% of its maximum value. This makes the type Ia supernovae to be calibrated standard candles and therefore they are very useful for cosmological

distance measurements. The apparent magnitude and the luminosity distance $d_L(z) = r(z)/a$, which is cosmology dependent, are related by

$$m(z) = M + 5\,log_{10}\left(\frac{d_L(z)}{1\,Mpc}\right) + 25 = \mathcal{M} + 5\,log_{10}\left(Q(z)\right) \tag{2.38}$$

where $Q(z) = d_L(z)H_0/c$ is the Hubble-constant-free luminosity distance and $\mathcal{M} = M - 5log_{10}h + 42.38$. It turned out that the observed type Ia supernovae were dimmer than expected for an Einstein de Sitter universe indicating that the (late) universe is undertaking an accelerated expansion since redshift $\simeq 0.4$. Observations can be fitted by the new Concordance ΛCDM cosmological model as it is shown in figure 2.3

The late time acceleration of the universe was pointed out early in Perlmutter et al. (1999) and any new compilation of supernovae data (eg. Riess et al. (2004)) have consistently found the same result. Obviously not only the supernovae data but the large scale structure (Allen et al. 2002) and the CMB (Spergel et al. 2003) support the Cosmological Concordance Model. In this section we have focused in supernovae because in chapter 6 we will use Tonry et al.' (2003) data as a consistency check for the model and in chapter 10 we will also use supernovae data together with Integrated Sachs Wolfe data to jointly constrain cosmological parameters.

Chapter 3

Growth of Structure in non-standard models: Methodology

Summary

In this chapter I present the formalism for computing the growth of structure in non-standard models. This formalism, which makes no explicit use of Einstein's equations, will be applied in the next three chapters to the DGP, the Cardassian and the Chaplygin gas models. Here I also present the Press-Schechter formalism used for cluster number counts predictions.

3.1 Growth of structure in non-standard cosmologies

In order to study the growth of structure in non-standard cosmologies we start with the Raychaudhuri's equation. We are interested in this equation because a) it holds without reference to Einstein's equations (which might not apply in non-standard cosmologies) and b) since it looks at the convergence of a congruence of geodesics it is easily related to the growth of perturbations. As mentioned in section 2.3, in the spherical collapse model (which implies no shear and no vorticity) we can write the Raychaudhuri's equation 2.16 as

$$\frac{\dot{\theta}}{a} + \frac{\theta}{a}\bar{H} + \frac{1}{3}\frac{\theta^2}{a^2} = 3(\dot{H} + H^2) - 3(\dot{\bar{H}} + \bar{H}^2). \tag{3.1}$$

Note again that up to this point we have not assumed anything other than we live in a FRW universe filled with dark matter. In particular, we have not assumed any connection between the geometry and the energy content but simply rewritten, in the spherical collapse model, the Raychaudhuri's equation in terms of the scale factor. This is useful since now we can study the evolution of the density perturbations armed with the Friedmann equation and the continuity equation, without having to concern us with the Einstein's equations. This is a genuine approach of this thesis and we will apply it to the Dvali Gabadadze Porrati, the Cardassian, and the Chaplygin gas models.

Following similar steps like in the standard case in section 2.3 we can express equation 3.1 in terms of density fluctuations and H. The result is

$$\frac{d^2\delta}{d\eta^2} + (2 + \frac{\dot{\bar{H}}}{\bar{H}^2})\frac{d\delta}{d\eta} - \frac{4}{3}\frac{1}{1+\delta}(\frac{d\delta}{d\tau})^2 = -3\frac{1+\delta}{\bar{H}^2}\Big((\dot{H} + H^2) - (\dot{\bar{H}} + \bar{H}^2)\Big), \tag{3.2}$$

where again $\eta = \ln(a)$. Obviously, for non-standard models, we cannot progress further unless the Friedmann equation and the continuity equation are known so that $\dot{H}$ can be calculated. If so, the $\dot{H}$, as well as, H^2 can be expressed in terms of the density contrast, δ, (just by doing $\rho = \bar{\rho}(1+\delta)$), the cosmological parameters (Ω_m,Ω_Λ,...) and the scale factor a. Subsequently, we have an equation that allow us to determine the growth of density fluctuations in terms of cosmological model-dependent parameters and a. It is convenient to expand the $\dot{H} + H^2$-term in terms of δ; then, the whole RHS of Eq. (3.2) is

$$3\frac{1+\delta}{\bar{H}^2}\Big((\dot{H} + H^2) - (\dot{\bar{H}} + \bar{H}^2)\Big) \equiv 3(1+\delta)\sum_{n=1} c_n\delta^n. \tag{3.3}$$

Note that there is no constant term in the expansion. It is obvious also that the coefficients c_n depend on the (non-standard model) cosmological parameters and a.

Expanding the perturbation according to Eq. (2.28) the linear equation is then

$$D_1'' + (2 + \frac{\dot{\bar{H}}}{\bar{H}^2})D_1' + 3c_1D_1 = 0, \tag{3.4}$$

the second order equation

$$D_2'' + (2 + \frac{\dot{\bar{H}}}{\bar{H}^2})D_2' - \frac{8}{3}(D_1')^2 + 3c_1D_2 + 6(c_1 + c_2)D_1^2 = 0 \tag{3.5}$$

and further orders are easily found. In the standard ΛCDM cosmology we get

$$c_1 = -\frac{4\pi G}{3}\frac{\bar{\rho}_m}{\bar{H}^2} = -\frac{1}{2}\frac{\Omega_M}{\Omega_M + a^3\Omega_\Lambda} \tag{3.6}$$

$$c_i = 0,\ i = 2, 3, ... \tag{3.7}$$

$$\frac{\dot{\bar{H}}}{\bar{H}^2} = -\frac{3}{2}\frac{\Omega_m}{\Omega_m + a^2\Omega_\Lambda} \tag{3.8}$$

Using these, the linear and second order equations, Eqs (2.29) and (2.33) are easily reproduced.

Note that in this formalism for non-standard Friedmann equation there is only (pressureless) dark matter fluctuations. In case that dark energy is present it is to be considered with no perturbations at all or with perturbations much smaller than the dark matter ones. This is, its role is only related to the expansion of the universe as expressed in the $\bar{H}$ and $\dot{\bar{H}}$ terms.

Equation 3.2 corresponds to the spherical collapse model and is the key equation for the growth of structure in the next three chapters. This equation is in fact equivalent to require that the underlying gravity theory respects the generalization of Birkhoff's law: for any test particle outside a spherically symetric matter source, the metric observed by that test particle is equivalent to that of a point source of the same mass located at the center of the sphere. This was shown by Lue et al (2004a). They computed, in the spherical collapse model and requiring the Birkhoff law to hold, the growth of perturbations of a dust like universe. Their equation of evolution (eq 4.5) turns out to be equivalent to our equation 3.2.

3.2 Cluster number counts

Cluster number counts is a promising tool in cosmology to discriminate among different dark energy models and to fit cosmological parameters. Several authors (Le Delliou 2006; Wang et al. 2004; Lima & Hu 2004; Haiman et al. 2000; Horellow & Berge 2005) have used the cluster number count together with other observable to show how future galaxy cluster surveys would constrain cosmological parameters like the amount of dark energy today or the equation of state parameter.

The redshift dependence of cluster number counts have already been used by Solevi et al. (2006) to investigate non-coupled quintessence models: SUGRA (Brax & Martin 1999) and RP (Ratra and Peebles 1988). In this thesis we use it to investigate coupled quintessence models as well as the

Cardassian and the Dvali-Gabadadze-Porrati models.

Both the Press-Schechter formalism and the Sheth and Tormen fit give a prediction for the comoving number density of collapsed halos of a given mass $n(m)$. We can integrate it if we want the density of clusters from above a mass threshold. Since we also want to compare with astronomical data it will be appropriate to convert $n(m)$ to a cluster number counts per redshift and square degree.

$$\frac{dN}{dz} = \int_{1deg^2} d\Omega \frac{dV}{dz d\Omega} \int_{M_{min}}^{\infty} n(M) dM \,. \tag{3.9}$$

Note that the comoving volume element per unit redshift, $dV/dz = d\Omega r(z)^2/H(z)$ with $r(z)$ being the comoving distance, depends strongly on the cosmological parameters and, as we will also see in chapter 7, on the coupling between dark matter and dark energy. Therefore it will play an important role on determining the total amount of cluster number counts in a given cosmological model. We will also see how the number counts depend strongly on the growth of structure.

3.2.1 Press-Schechter formalism

Press and Schechter formalism (Press & Schechter 1974) and its extensions (Bond J. et al. 1991; Lacey & Cole 1993) provides a prediction for the number density of collapsed objects. The main assumption in the Press and Schechter formalism is the gaussianity of the matter density field. When the density fluctuation field $\delta(\vec{x})$ is smoothed with a top hat window of radius R, i.e, when averaged in a sufficiently large volume $V = \frac{4\pi}{3}R^3$ around each point, it follows a Gaussian distribution:

$$p(\delta_L, R) = \frac{1}{\sqrt{2\pi}\sigma} e^{-\frac{\delta_L^2}{2\sigma^2}} \,, \tag{3.10}$$

where $\sigma(R)$ is the rms of linear fluctuations δ_L. Both $\sigma(R)$ and δ_L are redshift dependent. The volume fraction of points with $\delta_L \geq \delta_c$ is

$$\tilde{F} = \int_{\delta_c}^{\infty} p(\delta_L, R) d\delta_L = \frac{1}{2} \mathrm{erfc}\left(\frac{\delta_c}{\sqrt{2}\,\sigma(R)}\right) \,, \tag{3.11}$$

which is assumed to be equal to the mass fraction in bounded objects with $M \geq \frac{4\pi}{3}\rho_m R^3$. We have obviously integrated from δ_c, the critical density fluctuation required for the objects to have collapsed (see section 2.3.3, the spherical collapse model). For Einstein-de-Sitter cosmology $\delta_c = 1.686$ while

for other Λ CDMcosmologies there is a weekly dependence on Ω_m and Ω_Λ (see eg. (Eke et al. 1998) for ΛCDM and (Nunes & Mota 2006) for models with dark energy inhomogeneities).

We are interested in the comoving number density of collapsed objects in a mass range. To obtain this we have to take the derivative of $\tilde{F}$, which gives the mass fraction in objects with mass between M and $M + dM$, and also multiply by $\frac{\bar{\rho}}{M}$, which converts the result into number densities. Here $\bar{\rho}$ is the comoving matter density. Thus, the prediction of the Press-Schechter formalism for the comoving number density of collapsed objects is:

$$\begin{aligned} n(M)dM &= 2\frac{\bar{\rho}}{M}\frac{d\tilde{F}}{d\sigma}\frac{d\sigma}{dM}dM = \frac{\bar{\rho}}{M}\frac{dF}{d\sigma}\frac{d\sigma}{dM}dM \\ &= -\sqrt{\frac{2}{\pi}}\left(\frac{\delta_c}{\sigma}\right)\frac{d\ln\sigma}{d\ln M}\exp\left(-\frac{\delta_c^2}{2\sigma^2}\right)\frac{\bar{\rho}\,dM}{M^2},. \end{aligned} \tag{3.12}$$

This equation is called the unconditional mass function. Note that there is a factor of two ($F = 2\tilde{F}$) introduced to recover the mean matter density. This factor can be better understood when taking into account the 'cloud-in-cloud' structure of halos ((Bond J. et al. 1991)).

There seems to be some confusion in the literature regarding equation (3.12). It is worth to stress that the matter density $\bar{\rho}(z)$ in this equation is the *comoving* mean matter density at a given redshift. In most cases, it is constant and is equal to the *present* mean matter density, but not always. For instance, this equivalence is no longer true when one generalizes the Press-Schechter formalism to coupled quintessence models. In this case one has to bear in mind that $\bar{\rho}$ varies with redshift directly affecting the prediction of the number density of collapsed objects.

Following Vianna & Liddle (1999) we could take the variance in spheres of radius R to be

$$\sigma(R,z) = \sigma_8\left(\frac{R}{8h^{-1}Mpc}\right)^{-\gamma(R)}D(z)\,, \tag{3.13}$$

where D(z) is the growth factor and

$$\gamma(R) = (0.3\Gamma + 0.2)\left[2.92 + \log_{10}\left(\frac{R}{8h^{-1}Mpc}\right)\right], \tag{3.14}$$

where Γ is the shape parameter of the transfer function. As in (Sugiyama 1995), we want to take

into account the baryon component, thus having

$$\Gamma = \Omega_m h \exp\left(-\frac{\Omega_b(1+\sqrt{2h})}{\Omega_m}\right), \tag{3.15}$$

The Press-Schechter formalism as well as the fit in equation 3.14 could be crude for the present day precision cosmology. However it is still good enough and very useful formalism if one is not seeking exact solutions nor precise confrontations to observational data, but to understand the influence of different cosmological models in the cluster number counts predictions.

3.2.2 Sheth and Tormen fit

Several groups (Governato et al. 1999; Gross et al. 1998; Jenkins et al. 2001; Springel et. al. 2005) found significant deviations between N-body simulations and Press-Schechter predictions. The later producing less massive halos and more halos in the smaller mass range. A better fit to the simulations is given by Sheth & Tormen (1999) or Jenkins et al. (2001) fits to $n(m,z)$.

The Sheth and Tormen fit is

$$\begin{aligned} n(M)dM &= \frac{\bar{\rho}}{M}\frac{dF}{d\sigma}\frac{d\sigma}{dM}dM = \frac{\bar{\rho}}{M}\frac{dF}{d\nu}\frac{d\nu}{dM}dM \\ \frac{dF}{d\nu} &= A(p)\left(1+(q\nu)^{-p}\right)\left(\frac{q\nu}{2\pi}\right)^{1/2}\exp\left(-\frac{q\nu}{2}\right). \end{aligned} \tag{3.16}$$

where the normalization is given by

$$A(p) = \left[1 + \frac{2^{-p}\Gamma(1/2-p)}{\sqrt{\pi})}\right]^{-1} \tag{3.17}$$

When $p = 0$ and $q = 1$ we recover the Press-Schechter formula. Typical values for the fit are $p \simeq 0.3$ and $q \simeq 0.75$ (and therefore $A \simeq 0.3222$) (Sheth & Tormen 1999; Cooray & Sheth 2002). The parameter ν is defined as $\nu = \delta_c/\sigma^2$. At small $\nu << 1$, $dF/d\nu \propto \nu^{-(0.5+p)}$. While the small behavior of $dF/d\nu$ depends on the value of p, the exponential cutoff at $\nu >> 1$ does not. There is a characteristic scale mass, m_* defined by $\nu = 1$, i.e., $\sigma(m_*) \equiv \delta_c(z)$ (Cooray & Sheth 2002). At $z = 0$ this scale is $m_* \sim 2 \cdot 10^{13} M_{solar}/h$ and halos more massive that this are rare.

Chapter 4

Non standard cosmologies I:

The DGP model

Summary

In this chapter I present the brane induced gravity model of Dvali Gabadadze and Porrati (Dvali et al. 2000). Results for its linear and nonlinear growth of structure are shown as in Multamaki, Gaztanaga & Manera (2003).

4.1 The Dvali Gabadadze Porrati (DGP) model

The branewold induced gravity model (Dvali et al. 2000) offers an alternative explanation to the observed acceleration of the universe by means of a modification of gravity due to the presence of an extra dimension (Deffayet et al 2002a; Deffayet et al 2002b). Since, in this scenario, it is the slow leakage of gravity off our four dimensional world into an extra dimension what causes the late time acceleration, there is no need for a non-zero cosmological constant.

In the DGP model there is a characteristic scale, r_c which comes from the relation of the four and the five dimensions Plank Mass $r_c \equiv M_{4D}^2/2M_{5D}^3$. It is a free parameter of the theory and it is thought to be of order of the Hubble horizon. At large enough scales $r \simeq r_c$ gravity sees the full space-time, *i.e.*the brane *and* the bulk, and therefore the standard $1/r^2$ law for gravitational force

is substantially modified. In fact, in the large scale limit we would get a 5D gravity with a potential $V \propto 1/r^2$ instead of the well known $1/r$ form term of the 4D gravity.

Although we are here interested in cosmological perturbations (therefore relatively large scales), it is worth to mention that the DGP scenario might be also tested within solar system scales. At small scales the DGP potential has effectively added a repulsive logarithmic term to the gravitational potential which will give rise to an extra radial acceleration term. The possible testable effects are an extra secular precession of orbits of the planets (Lue & Starkmann 2003; Dvali et al. 2003; Iorio 2005) or the increase increase of the Astronomical Unit (Iorio 2005).

In the DGP-scenario the Friedmann equation on the brane is (Deffayet et al 2002a):

$$H^2 = \Big(\sqrt{\frac{8\pi G}{3}\rho + \frac{1}{R^2}} + \frac{1}{R}\Big)^2 + \frac{K}{a^2}, \tag{4.1}$$

where $R \equiv 2r_c$ and $K = 0, \pm 1$ is the curvature constant. The evolution of the scale factor is standard as long as the energy density of matter dominates *i.e.* $\frac{8\pi G}{3}\rho \gg 1/R^2$. Since ρ decreases with time due to the expansion of the universe, the R^{-2} term becomes dominant at some point, and acting as an effective cosmological constant, it leads to an accelerating universe. At late times the scale factor grows exponentially, $a \sim \exp(t/R)$. The continuity equation $\dot{\rho} + 3H(\rho + p) = 0$ is unchanged.

We are interested in the growth of large scale structure which takes place in a matter dominated universe and hence we assume that $\rho \gg p$ and therefore $\rho \sim a^{-3}$. We can view the DGP-scenario as standard cosmology with a perfect fluid with the normal properties. The only difference is the non-standard Friedmann equation, which can be written as

$$H^2 = H_0^2\Big((\sqrt{\frac{\Omega_M}{a^3} + \Omega_R} + \sqrt{\Omega_R})^2 + \frac{\Omega_K}{a^2}\Big). \tag{4.2}$$

where we defined the cosmological parameters as usual:

$$\Omega_M \equiv \frac{8\pi G\rho_0}{3H_0^2} \tag{4.3}$$

$$\Omega_R \equiv \frac{1}{R^2H_0^2} \tag{4.4}$$

$$\Omega_K \equiv \frac{K}{H_0^2}, \tag{4.5}$$

where H_0 is the current Hubble rate and ρ_0 the current density of matter. Note that the normalization condition differs from the usual one,

$$1 = \left(\sqrt{\Omega_M + \Omega_R} + \sqrt{\Omega_R}\right)^2 + \Omega_K. \tag{4.6}$$

Now assuming that we we live in a flat universe, $K = 0$, so that Friedmann equation can be written as:

$$H^2 = H_0^2\Big(\frac{\Omega_M}{a^3} + 2\Omega_R(1 + \sqrt{1 + \frac{\Omega_M}{\Omega_R a^3}})\Big). \tag{4.7}$$

The normalization condition simplifies to

$$\Omega_M + 2\sqrt{\Omega_R} = 1, \tag{4.8}$$

from where it is clear that in order to have $\Omega_M > 0$, Ω_R must be restricted to the range $0 \leq \Omega_R < \frac{1}{4}$.

In Deffayet et al. (2002a) this model was tested with SNIa and the CMB data. It was found that the model is in agreement with data and the preferred parameter values for a flat universe are

$$\Omega_M = 0.18^{+0.07}_{-0.06},\ \Omega_R = 0.17^{+0.03}_{-0.02}. \tag{4.9}$$

Other groups have also tested DGP models with SNIa. Avelino & Martins (2002) used SNIa, CMB and cluster data and argued that the DGP model is disfavoured unless $\Omega_m \simeq 0.2$, which is actually near the best fit value of Deffayet et al. (2002a). Another test (Guo et al. 2006) shows that when fitting together SNIa and Baryon Acoustic Oscillations from SDSS the best fit value ($\Omega_m \simeq 0.27$) would require a closed universe, being a flat one still compatible at three sigma level. Since the constraints on DGP model from these studies are not strong enough to exclude the model

as an alternative to the Λ CDM cosmology it is worth to investigate if it is compatible with large scale structure. That is what we will do in the next two sections.

4.2 Growth of structure in DGP models

The DGP model can be thought as a modified Friedmann equation model. We can use the Friedmann equation and the continuity equation and compute the growth of structure. For this model we get

$$\dot{H} + H^2 = -\frac{3}{2}\kappa^2(1 + \frac{1}{R\sqrt{\kappa^2\rho + \frac{1}{R^2}}})(\rho + p) + \kappa^2\rho + \frac{2}{R}\sqrt{\kappa^2\rho + \frac{1}{R^2}} + \frac{2}{R^2}. \tag{4.10}$$

This is obviously different from the result that one gets in the standard case, $-\frac{4\pi G}{3}(\rho+3p)+\frac{\Lambda}{3}$, with the standard Einstein's equations. Thus, it is obvious that in the DGP-scenario the Raychaudhuri's equation needs to be calculated directly using the general approach described in the subsection 3.1.

In the matter dominated DPG-scenario:

$$\frac{1}{H^2}(\dot{H} + H^2) = \frac{\Omega_M\left(\sqrt{\Omega_R} - \sqrt{\frac{\Omega_M}{a^3} + \Omega_R}\right) + 4\,a^3\,\Omega_R\left(\sqrt{\Omega_R} + \sqrt{\frac{\Omega_M}{a^3} + \Omega_R}\right)}{2\,a^3\sqrt{\frac{\Omega_M}{a^3} + \Omega_R}\left(\sqrt{\Omega_R} + \sqrt{\frac{\Omega_M}{a^3} + \Omega_R}\right)^2}. \tag{4.11}$$

The coefficients c_i are easily calculated and the first two are, again expressed in cosmological quantities:

$$\begin{aligned} c_1 &= -\frac{2\left(\Omega_M + \Omega_R\,a^3\right)\left(\Omega_M + 4\,\Omega_R\,a^3\right) + \sqrt{\Omega_R}\sqrt{\Omega_R + \frac{\Omega_M}{a^3}}\,a^3\left(5\,\Omega_M + 8\,\Omega_R\,a^3\right)}{4(\Omega_M + \Omega_R\,a^3)^2} \\ c_2 &= \frac{\Omega_M^2\sqrt{\Omega_R}\sqrt{\Omega_R + \frac{\Omega_M}{a^3}}\left(8\Omega_R\,a^3 - \Omega_M\right)}{16\left(\sqrt{\Omega_R} + \sqrt{\Omega_R + \frac{\Omega_M}{a^3}}\right)^2(\Omega_M + \Omega_R\,a^3)^3}. \end{aligned}$$

Finally, we need to calculate the term appearing in front of the δ'-term in the perturbation equation (3.2):

$$2 + \frac{\dot{H}}{H^2} = \frac{1}{2} + \frac{3\sqrt{\Omega_R}}{2\sqrt{\Omega_R + \frac{\Omega_M}{a^3}}}. \tag{4.12}$$

Clearly, in the limit $\Omega_R = 0$, all these expressions reduce to the corresponding expressions in the

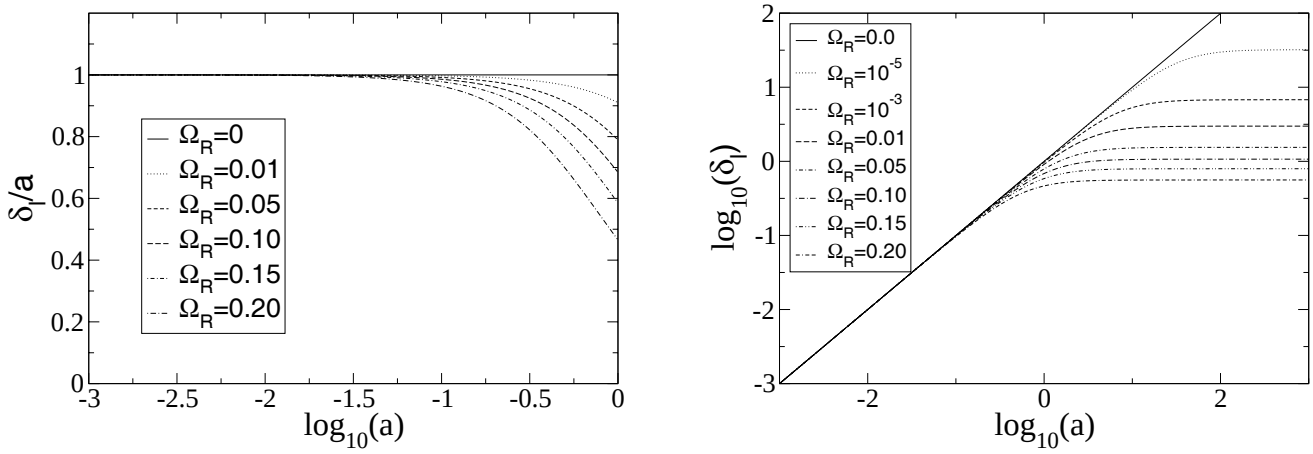

Figure 4.1: Linear growth for different values of Ω_R. Figure from Multamaki, Gaztanaga & Manera (2003).

Einstein-de-Sitter case.

4.2.1 Linear Growth

We can now study the growth of perturbations numerically. The initial conditions are chosen such that at $a = 10^{-3}$, the standard exponential solution, $D_1 \sim \exp(\eta)$, is reached. In Fig. 4.1 the linear growth factor (and the linear growth factor normalized with the scale factor) for different values of Ω_R, with Ω_M then determined by Eq. (4.8), are shown as a function of the scale factor.

The general form of the linear growth factor is similar to the cosmological constant case but here the effect is even more pronounced. For the preferred value $\Omega_R = 0.17$ (Dvali et al. 2003), the growth of linear fluctuations up to now is suppressed by a factor of 0.54 compared to the EdS-case. In the Λ-universe with $\Omega_\Lambda = 0.7$, the suppression is 0.78. Hence, there will be significantly less structure growth on large scales in the DGP-scenario than in a Λ-cosmology.

Normalization amplitude: σ_8

The amplitude of density fluctuations is commonly characterized by the linear value of the rms fluctuations on a sphere of $8Mpc/h$. Observationally its value seems to be of order unity at $z = 0$. Form the analysis in the previous sections it is straight forward to predict how different σ_8 should

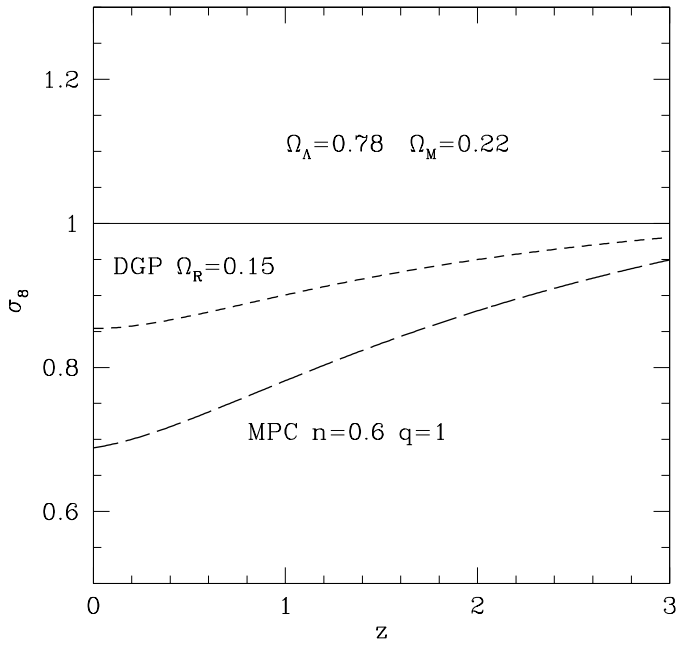

Figure 4.2: Value of σ_8 in DGP and Cardassian cosmologies, with $\Omega_M = 0.22$, relative to the value for the $\Omega_\Lambda = 0.78$, $\Omega_M = 0.22$ standard cosmology with $\sigma_8 = 1$. Figure from Multamaki, Gaztanaga & Manera (2003)

be for a given cosmological model. One way to do this is to fix the normalization of all models to be equal at high red-shifts and see how different they are at $z = 0.5$.[1] Figure 4.2 illustrates this point. We show the value of σ_8 normalized to the Λ model as a function of red-shift for DGP with $\Omega_m = 0.22$. The σ_8 is also plotted for the Cardassian model (see section 5.1). Values of σ_8 for other parameters can readily be obtained by comparing Figure 2.1 with Figure 4.1

Current observational constraints of σ_8 usually come with several different assumptions. In most cases a shape for the linear spectrum is assumed to get an estimation, for example from cluster abundances or normalization of CMB fluctuations. If the primordial spectrum of fluctuations is not scale invariance or a simple power-law, such extrapolations could yield misleading values of σ_8 (Barriga et al. 2001). Large scale structure in local galaxy catalogues also yield values $\sigma_8 \simeq 1$,

[1] In principle, this is similar to a CMB normalization, but note that in general a CMB normalization also requires some additional information on the shape of the spectrum, which might vary from model to model. Thus, here we choose to illustrate how σ_8 changes due to the linear growth from a given fixed shape of the spectra.

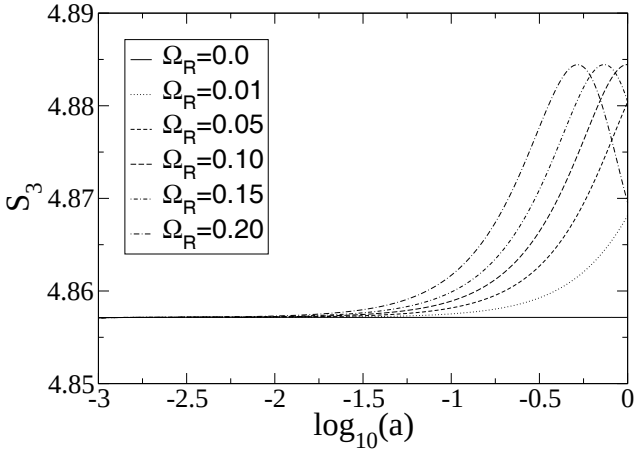

Figure 4.3: Non-linear growth for different values of Ω_R. Figure as in Multamaki, Gaztanaga Manera (2003)

but one needs to quantify the bias b, or how well the selected galaxies trace the underlying mass distribution (see e.g. Gaztanaga 1995). CMB Results from the *WMAP* (Spergel et al. 2003) mission fit to the (power-law) ΛCDM cosmology find: $\sigma_8 = 0.9 \pm 0.1$ More recent results from WMAP alone (Spergel et al. 2006) lower the σ_8 value to 0.75 ± 0.06 These values have been extrapolated from $z \simeq 10^3$ to $z = 0$ by using the linear growth factor $D_1(z)$ in Eq. (2.32). Significantly smaller values ($\sigma_8 \simeq 0.6 - 0.7$) have been found at low red-shifts by weak lensing (see for instance Jarvis et al. 2003), and by velocity fields investigations (see eg. Willick & Strauss 1998). This apparent discrepancy, if real, could be easily accounted for by using the DGP cosmological models (and also by Cardassian models).

4.2.2 Nonlinear growth

In calculating the second order perturbation, initial conditions are chosen such that the standard solution, constant $S_3 = \frac{34}{7} \approx 4.86$ is valid from the beginning. The non-linear growth is shown in Fig.4.3. The second order perturbation, or S_3, also grows differently from the Λ-cosmology. The value of S_3 starts to grow at earlier times and varies more than in the standard Λ-universe. However, the variation is still observationally insignificant being at best less than one percent.

The values shown in 4.3 are the unsmoothed values of the skewness at a single point. In practice,

to relate to observations, one needs to take into account smoothing effects. For a top-hat window of a given radius R, smoothing results in a simple linear correction that is given by the slope γ of the variance smoothed at a radius R (Juszkiewicz et al. 1993). In the standard cosmology: $S_3 = 34/7+\gamma$ (eg see Bernardeau et al. 2002 and references therein). The smoothing correction should be the same for non-standard cosmologies, as long as we work within the spherical collapse model (ie the shear-free approximation in Eq. (2.14)), which gives the exact leading order contribution to S_3 for a top hat window (Fosalba & Gaztanaga 98; Bernardeau et. al. 2002). Thus, the difference between the standard predictions and the predictions from non-standard cosmologies should not be affected by these smoothing effects. Besides smoothing effects, S_3 is also affected by systematic uncertainties of biasing (see §7.1 in Bernardeau et al. 2002).

Current estimations for S_3 (see §8 in Bernardeau et al 2002) agree with the standard predictions but with large uncertainties, of order $20\% - 30\%$. Thus current observations on S_3 can not be used to separate the different models.

As we have seen in section 3.2 the cluster number counts could be a nonlinear growth test for discriminating between non-standard cosmological models. For the DGP model we have plot the number density of clusters of mass $M > 2 \cdot 10^{14} M_{solar}$ per square degree and compared it to the Λ CDM prediction. As it is shown in figure 5.3 and the accompanying discussion the DGP model predicts about two times more clusters at redshift $z \simeq 1.5$ than the Λ CDM model.

We can compare the growth of structure as computed in this chapter (which was presented in Multamaki Gaztanaga & Manera 2003) with the results of Lue, Scoccimarro & Starkman (2004). Instead of using the equation 3.2 or requiring the Birkhoff's theorem to approximate the structure formation (both being equivalent), they have started with the 5D metric in the DGP model. For non-relativistic sources and under the assumptions that the overdensities do not alter the background cosmology and that the geodesic equation reduces appropriately to Newton's second law, they have found the linear growth in the DGP model to be equivalent to change the Newton's constant to an effective one. The effective Newton's constant in the Lue, Scoccimarro & Starkman (2004) paper is $G_{eff} = \frac{2+4\Omega_m^2(z)}{3(1+\Omega_m^2(z))}$. This produces a linear growth suppression compared to the ΛCDM model which is of order twice the value obtained in this chapter. Regarding the skewness they found the change respect to the EdS value to be as well of less than 1%.

Chapter 5

Non standard cosmologies II: The Cardassian model.

Summary

In this chapter I introduce the Cardassian model (Freese & Lewis 2002) and show results for its growth of structure. Most of this work is presented as in Multamaki, Gaztanaga & Manera (2003)

5.1 Cardassian models

In the Cardassian [1] models (Freese & Lewis 2002; Freese 2005) the universe is assumed to be flat with only matter and radiation components, and with no cosmological constant. The Friedmann equation has the general form

$$H^2 = g(\rho), \tag{5.1}$$

where the ρ is the energy density of ordinary matter and radiation. The function g is assumed to approach the standard form, $8\pi G\rho/3$ at early times, including nucleosynthesis, and at late times, $z < \mathcal{O}(1)$, to give accelerated expansion in accordance with the supernova observations (Perlmutter et al. 1999). Since the behavior of the function is different at different values of ρ, there is an associated scale, ρ_C, or redshift, z_{eq}, in the function g that determines when the evolution is standard and

[1] The Cardassian is an humanoid-like race from Star Trek, see e.g. www.startrek.com

when the non-standard terms begin to dominate. There are different Cardassian models according to the exact functional form of g, which can obviously vary as long as it satisfies the aforementioned constraints. Below we present the original Cardassian model and the Modified Polytropic Cardassian model. For completeness we will comment briefly on the less common suggestion of the exponential Cardassian model (Liu et al. 2006).

5.1.1 The original Cardassian model

The original Cardassian form of $g(\rho)$ (Freese & Lewis 2002) is:

$$H^2 = \frac{8\pi G}{3}\rho + B\rho^n,\ n < \frac{2}{3}. \tag{5.2}$$

At early times the universe is dominated by the first term (provided that B is small enough at the time of interest) and at late times the ρ^n-term becomes significant, providing acceleration compared to the standard case. The term of the form ρ^n in the Friedmann equation, and hence the Cardassian model(s), is motivated by considering our universe as a brane embedded in extra dimensions (Chung & Freese 2000) (this idea was, however, critically reviewed in Cline & Vinet (2003). A second possible interpretation of Cardassian model has been also developed (Gondolo & Freese 2003). It treats the modified Friedmann equations as due to a fluid, in which the energy density has new contributions with negative pressure. It is thought that this contributions might arise from matter self-interactions.

The requirement that $n < \frac{2}{3}$ comes from demanding an accelerated expansion. It is actually more universal requirement as one can see from considering the acceleration of the scale factor from the general Cardassian form, Eq. (5.1):

$$\frac{\ddot{a}}{a} = g(\rho) - \frac{3}{2}\rho g'(\rho), \tag{5.3}$$

where it has been assumed the usual continuity equation for matter $p = 0$, $\dot{\rho} + 3H\rho = 0$. If we wish to have late time acceleration, $\ddot{a}/a$ must be greater than zero, and hence at late times the inequality

$$g(\rho)_{late} < B\rho^{\frac{2}{3}} \tag{5.4}$$

must hold. Therefore, in order to have late time acceleration, the Cardassian function, $g(\rho)$, must grow more slowly than $\rho^{\frac{2}{3}}$ at late times.

The Friedmann equation (5.2) can be written in terms of the scale ρ_C, which determines when the non-standard term starts to dominate.

$$H^2 = \frac{8\pi G}{3}\rho[1 + (\frac{\rho}{\rho_C})^{n-1}], \tag{5.5}$$

Here $B = \frac{8\pi G}{3}\rho_C^{1-n}$. In a matter dominated universe this is conveniently parameterized by the redshift at which the two terms are equal, z_{eq},

$$H^2 = \frac{8\pi G}{3}\rho[1 + (1 + z_{eq})^{3(1-n)}(\frac{\rho}{\rho_0})^{n-1}], \tag{5.6}$$

where ρ_0 is the current energy density of matter.

The original Cardassian model has been constrained in several works. Zhu & Fujimoto (2002) considered the angular size of compact radio sources at different redshifts. Zhu & Fujimoto (2003,2004) used type Ia supernovae. And CMB data have been also used by Sen & Sen (2003a,2003b).

5.1.2 The Modified Polytropic Cardassian model

The Modified Polytropic Cardassian (MPC) model is an extension of the original Cardassian model that have also been studied with SNIa observations (Wang et al. 2003). This model has the following Friedmann equation:

$$H^2 = \kappa^2\rho[1 + \left(\frac{\rho}{\rho_C}\right)^{q(n-1)}]^{1/q}, \tag{5.7}$$

Here ρ_C is again the energy density of matter at which the non-standard terms begin to dominate and $q > 0$ is a new added parameter[2]. The original Cardassian model is a special case of the MPC model with q=1 and hence in this thesis we will concentrate on this more general model.

The Friedmann equation in the MPC-scenario in a matter dominated universe can equally be written in terms of the redshift at which the Cardassian terms start to dominate:

$$H^2 = H_0^2\frac{\Omega_M}{a^3}\left(1 + (1 + z_{eq})^{3(1-n)q}a^{3(1-n)q}\right)^{\frac{1}{q}} \tag{5.8}$$

[2]Incidentally, the Q-continuum is another race from Star Trek, existing in extra dimensions (www.startrek.com)

In a flat universe, which is the case we want to consider, the observed matter density of the universe, Ω_M, can be related to z_{eq} by

$$1 + z_{eq} = [(\Omega_M^{obs})^{-q} - 1]^{1/(3q(1-n))}. \tag{5.9}$$

The MPC-model is constrained by the supernova observations as well as the CMB (Wang et al. 2003). The experimentally allowed (n, q) parameter space is large and there is a degeneracy along the q axis at for $q \geq 10$ (when $\Omega_M = 0.3$) (Wang et al. 2003).

5.1.3 The exponential Cardassian model

The exponential Cardassian model is a new model recently presented in the literature (Liu et al. 2006). Although we are not studying it in this thesis we mention it briefly just for completeness. The Friedmann equation in this model is

$$H^2 = \frac{8\pi G}{3}\rho \exp\left[\left(\frac{\rho_{ca}}{\rho}\right)^n\right] \tag{5.10}$$

where ρ_{ca} is a characteristic energy density constant of the model. For having an accelerated expansion of the universe it is required that $3n(\rho_{ca}/\rho_0)^n > 1$ where ρ_0 is the current matter energy density. This model is consistent with type Ia supernovae data and might be motivated because of its equation of state parameter for an effective dark energy fluid can naturally cross the phantom divide $w = -1$ without introducing 'exotic' dark energy.

5.2 Growth in the Cardassian Model

In this section we will consider the growth of the perturbations in the Cardassian model. Since we are in a modified Friedmann equation model we will follow section 3.1 and find the growth of perturbations from using the continuity and the Friedmann equations. In this framework we consider with vanishing pressure. This framework differ from Gondolo & Freese (2003) where the dark matter has negative pressure.

Initial conditions are chosen as in the DGP model, they are such that at $a = 10^{-3}$, the standard Λ CDM exponential solution, $D_1 \sim \exp(\eta)$, is reached. In calculating the second order perturbation,

initial conditions are chosen such that the standard solution, constant $S_3 = \frac{34}{7} \approx 4.86$ is valid from the beginning.

5.2.1 Perturbations in the Original Cardassian model

For the original Cardassian model the coefficients of the differential equations we want to solve are:

$$c_1 = \frac{-\frac{1}{2} + n(1-\frac{3}{2}n)(1+z_{eq})^{3(1-n)}a^{3(1-n)}}{1+(1+z_{eq})^{3(1-n)}a^{3(1-n)}} \tag{5.11}$$

$$c_2 = \frac{\frac{1}{2}n(n-1)(1-\frac{3}{2}n)(1+z_{eq})^{3(1-n)}a^{3(1-n)}}{1+(1+z_{eq})^{3(1-n)}a^{3(1-n)}} \tag{5.12}$$

$$2+\frac{\dot{H}}{H^2} = 2-\frac{3}{2}\frac{1+n(1+z_{eq})^{3(1-n)}a^{3(1-n)}}{1+(1+z_{eq})^{3(1-n)}a^{3(1-n)}}. \tag{5.13}$$

Again, as a check it is easy to see that with $n = 0$, we recover the standard coefficients (3.6). We can now calculate the growth of perturbations in the original Cardassian scenario $q = 1$

Linear growth

The equation determining linear growth, Eq. (3.4), in the Cardassian model in a scaled form is

$$\frac{d^2D_1}{dx^2} + \Big(2-\frac{3}{2}\frac{1+ne^{3(1-n)x}}{1+e^{3(1-n)x}}\Big)\frac{dD_1}{dx} + \frac{3}{2}\frac{2n(1-\frac{3}{2}n)e^{3(1-n)x}-1}{e^{3(1-n)x}+1}D_1 = 0, \tag{5.14}$$

where $x \equiv \ln(a/a_{eq}) = \eta - \eta_{eq}$.

The solution to the linear equation in the original Cardassian model can be expressed in terms of the hypergeometric function. The growing part of the solution is found to be

$$D_1(x) = e^x {}_2F_1\Big[1, \frac{2+3n}{6(1-n)}, \frac{11-6n}{6(1-n)}, -e^{3(1-n)x}\Big],\ n < \frac{2}{3}. \tag{5.15}$$

The linear growth is plotted in figure 5.1. As we will deduce just below the slowest growth corresponds to $n = \frac{4}{9}$. In figure 4.2 we have also plotted the fluctuations normalization amplitude σ_8 relative to the Λ CDM model for the original Cardassian model with n=0.6 and for the DGP model. It can be seen that, if we normalize all models to have the same growth factor at the past, their σ_8 differ today, being 25% less for the Cardassian model than for the concordance Λ CDM model. Other values for σ_8 can be obtained comparing figure 5.1 (or figure 5.4 for the generalized

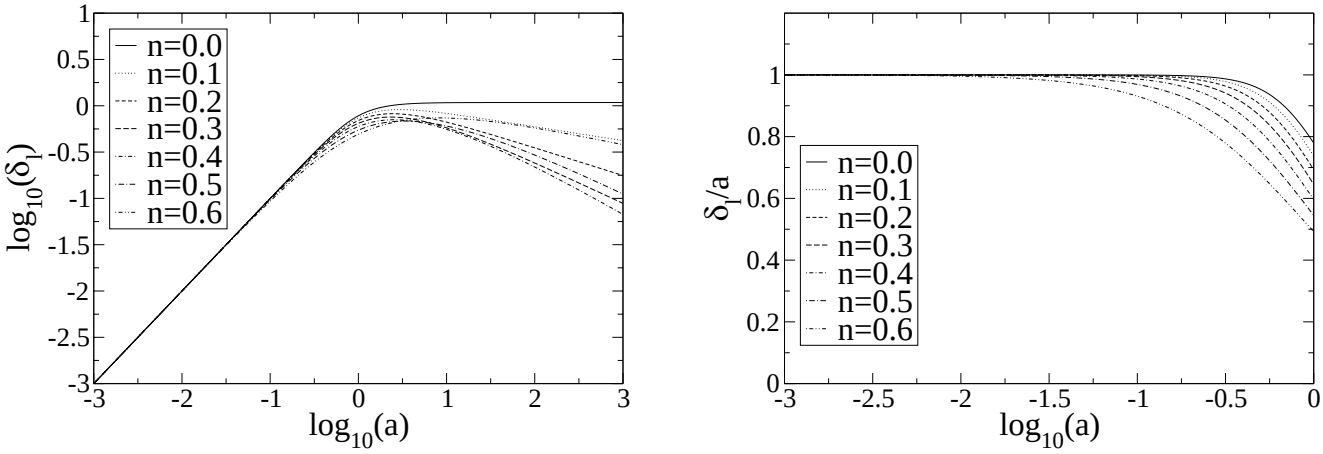

Figure 5.1: Linear growth for different values of n in the original Cardassian model $q = 1$. We set $\Omega_M = 0.3$. Figures as in Multamaki, Gaztanaga & Manera (2003).

case) with figure 2.1. Note that with $q \neq 1$ we can also get $\sigma_8 > 1$

For the general case, no analytical solution is found for the linear and nonlinear growth.

It is now interesting to look at the large $|x|$ limits. Since we are interested in the range of values where $0 < n < \frac{2}{3}$, it is clear that, depending on the sign of x, the exponential terms in Eq. (5.14) will either dominate or be negligible in the large x limit. When x is large and negative, *i.e.*when $a/a_C \ll 1$, Eq. (5.14) takes the form

$$\frac{d^2D_1}{dx^2} + \frac{1}{2}\frac{dD_1}{dx} - \frac{3}{2}D_1 = 0, \tag{5.16}$$

*i.e.*the standard form, which has the usual solution

$$D_1^-(x) = A_1 e^x + A_2 e^{-\frac{3}{2}x}. \tag{5.17}$$

In the large positive x-limit, *i.e.*when $a/a_C \gg 1$, it is obvious that the exponential terms will dominate and so that Eq. (5.14) can be written as

$$\frac{d^2D_1}{dx^2} + (2 - \frac{3}{2}n)\frac{dD_1}{dx} + 3n(1 - \frac{3}{2}n)D_1 = 0. \tag{5.18}$$

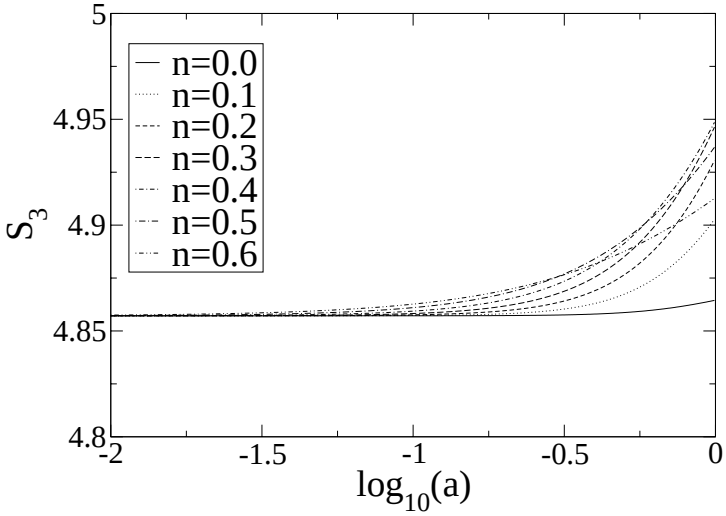

Figure 5.2: Non-linear growth for different values of n in the original Cardassian model $q = 1$. We set $\Omega_M = 0.3$. Figure as in Multamaki, Gaztanaga & Manera (2003).

The solution to this equation is easily found and reads as

$$D_1^+(x) = B_1 e^{-\frac{3}{2}nx} + B_2 e^{(3n-2)x}, \tag{5.19}$$

where B_i are constants. Looking at the solutions, we see that with $n = 1$, the two solutions agree as expected. If $n < \frac{2}{3}$, the linear growth of perturbations will at some point stop and perturbations start to shrink.

The slowest growth rate at large a/a_{eq} is easily deduced from $D_1^+(x)$ and occurs when $-\frac{3}{2}n = 3n - 2$, *i.e.*, when $n = \frac{4}{9}$ and hence $D_1^+(x) \sim e^{-\frac{2}{3}x}$.

5.2.2 Second order perturbations

The second order perturbations for the original Cardassian model and different values of n are shown in figure 5.2

We can also look at the $|x|$ limits. The equation determining the growth of second order perturbations in the large x limit (in the negative large x limit we obviously reproduce the standard

scenario again) is from Eq. (3.5),

$$\frac{d^2D_2}{dx^2} + (2 - \frac{3}{2}n)\frac{dD_2}{dx} + 3n(1 - \frac{3}{2}n)D_2 - \frac{8}{3}\Big(\frac{dD_1}{dx}\Big)^2 + 3n(n+1)(1 - \frac{3}{2}n)D_1^2 = 0. \tag{5.20}$$

The part that will dominate the linear solution D_1 depends on n, if $n < \frac{4}{9}$, $D_1 \sim \exp(-\frac{3}{2}nx)$, where as if $\frac{4}{9} < n < 1$, $D_1 \sim \exp((3n-2)x)$. Let us first assume that $n < \frac{4}{9}$, in which case by substituting the appropriate solution of D_1 into Eq. (5.20) and solving the resulting equation, we get

$$D_2(x) = \frac{1}{2}(2+n)e^{-3nx} + C_1 e^{-\frac{3}{2}nx} + C_2 e^{(3n-2)x}. \tag{5.21}$$

Hence, since $n < \frac{4}{9}$, we see that in the large x limit, $D_2 \sim e^{-\frac{3}{2}nx}$. Therefore, we expect that in this limit,

$$S_3 \sim e^{\frac{3}{2}nx}. \tag{5.22}$$

If we instead look at the values of $\frac{4}{9} < n < 1$, we see that $S_3 \sim e^{(2-3n)x}$, and hence the value of n that gives the largest effect rate of change of S_3 is, again, at $n = \frac{4}{9}$ with $S_3 \sim e^{\frac{2}{3}x}$.

Cluster number counts

As we have seen in section 3.2 the Press-Schechter formalism allow us to predict the evolution the mass function of collapsed objects (halos or clusters). This is an increasingly powerful tool to discriminate between non-standard models and the Λ CDM cosmology. In figure 5.3 we plot the number density of predicted clusters per square degree with a mass $M > 2 \cdot 10^{14} M_{solar}$ for the Cardassian model and for the DGP model as well.

Note that there are four important factors in the PS predictions: i) Ω_M, which relates a given cluster mass M to R in $\sigma(R)$ value in eq 3.12 ii) the shape of the power spectrum, which determines the $\sigma(R)$ curve, iii) the volume element, which we plot in the bottom part of figure 5.3, and iv) the growth factor in units of the critical mass density fluctuation $D_1(z)/\delta_c(z)$ which gives the red-shift variation of σ.

When analysing the Cardassian and DGP models we have fixed i) and ii) to the Λ cosmology with $\Omega_M \simeq 0.22$. For simplicity we have also fixed $\delta_c(z)$ to the Einstein-de-Sitter value $\delta_c = 1.686$ because we find little difference of this value in the models. Thus, all differences in figure 5.3 are

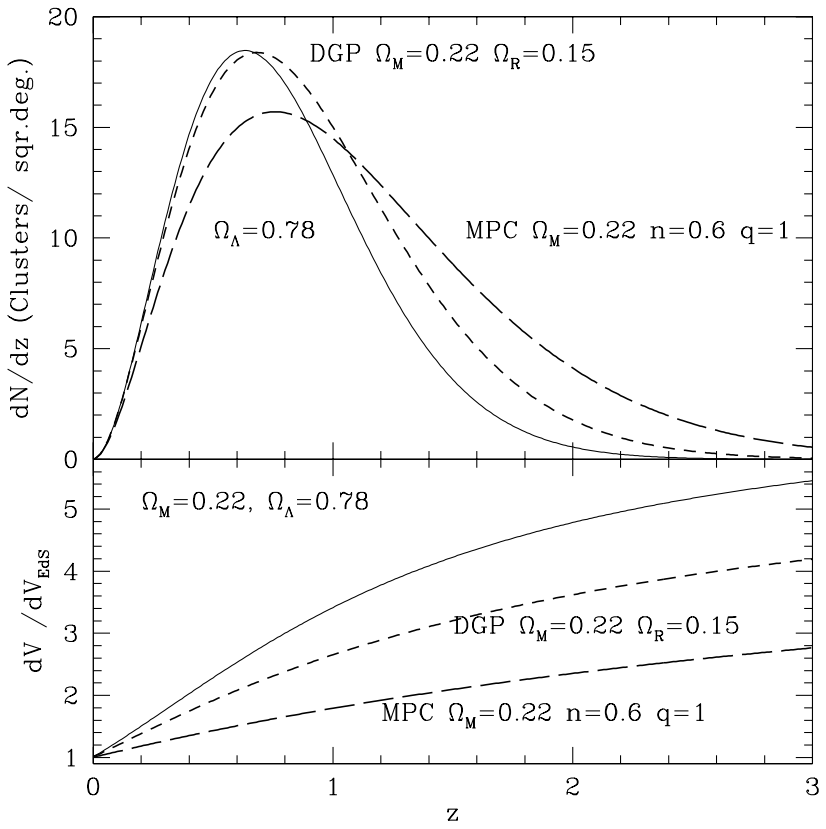

Figure 5.3: Bottom: Comoving volume element as a function of red-shift normalized to the EdS model. The short and long dashed line shows DGP and MPC predictions for $\Omega_M = 0.22$ ($\Omega_R = 0.15$) and $h = 0.71$. The continuous line corresponds to the Λ cosmology with $\Omega_M = 0.22$ ($\Omega_\Lambda = 0.78$) and $h = 0.71$. Top: Number density of predicted clusters per square degree with mass $M > 2{\times}10^{14} M_{solar}$ for the same models. All models are normalized to $\sigma_8 = 1$ at $z = 0$. Figure from Multamaki, Manera & Gaztanaga (2003).

due to differences in volume and growth factors, which mark the distinction between standard and most non-standard cosmologies.

The growth factor is already plotted in the linear growth figures for those models. We plot the volume element dV/dz normalized to the standard case in the bottom part of figure 5.3 As can be seen in the figure, the Λ cosmology has about 4 times more comoving volume by $z \simeq 1.5$ than the EdS case, while DGP and MPC are only 3 and 2 times larger. Despite the smaller volumes, DGP and MPC predicts 2 and 4 times more clusters at $z \simeq 1.5$ than the Λ cosmology because of the stronger freeze in the linear growth factor, which can be seen by comparing Figure 2.1 to Figure 4.1.

5.2.3 Perturbations in the Modified Polytropic Cardassian model

Using the Friedmann equation and the continuity equation we compute the term $\dot{H} + H^2$ in the MPC model

$$\frac{1}{H^2}(\dot{H} + H^2) = -\frac{1}{2}\frac{1 + (1+z_{eq})^{3(1-n)q}(3n-2)(\frac{\rho}{\rho_0})^{(n-1)q}}{1 + (1+z_{eq})^{3(1-n)q}(\frac{\rho}{\rho_0})^{(n-1)q}} \tag{5.23}$$

Then we can get the first two c_i coefficients

$$c_1 = -\frac{1}{2}\frac{1 + (4n - 2 + 3(n-1)^2 q)X + n(3n-2)X^2}{\Big(1+X\Big)^2} \tag{5.24}$$

$$c_2 = \frac{X}{4}(1+X)^{-3}(n-1)\Big[\Big((1-n)q - 1\Big)\Big(1 + 3(n-1)q\Big) \tag{5.25}$$

$$+\Big(2 - 4n - (n-1)(9n-5)q + 3(n-1)^2 q^2\Big)X + n(2-3n)X^2\Big], \tag{5.26}$$

where we have defined $X \equiv ((1+z_{eq})a)^{3(1-n)q}$ in order to shorten the otherwise lengthy expressions.

Finally, in order to study the growth of perturbations, we need the coefficient of the δ' term in 3.2:

$$2 + \frac{\dot{\dot{H}}}{H^2} = 2 - \frac{3}{2}\frac{1 + n(1+z_{eq})^{3q(1-n)}a^{3q(1-n)}}{1 + (1+z_{eq})^{3q(1-n)}a^{3q(1-n)}}. \tag{5.27}$$

We have solved numerically the differential equation for D and plotted the linear an nonlinear growth (the skewness) in figures 5.4 and 5.5 Results are shown for $n = 0, 0.1, ..., 0.6$ and $q = 2, 5, 10$. The $q = 1$ case had been displayed before in section 5.2.1 since it corresponds to the Original Cardassian model. The linear growth factor is presented both on a logarithmic scale and scaled by

the scale factor. In plotting these figures, we have assumed that $\Omega_M = 0.3$, which then sets the value of z_{eq} according to Eq. (5.9).

From the figures it is clear how the Cardassian scenario is fundamentally different from the Λ CDM and the DGP models. Looking at the behavior of the linear growth when $n > 0$ (since $n = 0$ corresponds to a cosmological constant) we see that it actually begins to decrease in the future, *i.e.*, areas of higher density begin to rarify. This is true regardless of the value of q. Near the turning point there is some interesting behavior as is visible from the plots of δ_l/a. With larger values of q we see that before the growth factor starts to decrease, structures grow more rapidly compared to the standard case. This was seen neither in ΛCDM nor in the DGP model. The value of δ_l/a at present is dependent on the value of the parameters but can be as small as 0.5.

Looking at the figures depicting the change in S_3, figs 5.4 and 5.5, we see that in the Cardassian model the evolution of the value of S_3 is strongly dependent on the value of q. The shape and the magnitude of variation changes with q so that with larger q one sees larger variations.

In the original Cardassian scenario, figure 5.2, the values of S_3 grow faster compared to the EdS scenario. The overall shape of the curves is similar to that of the standard $\Lambda \neq 0$ universe described in section 2.3. However, here the scale of the change in S_3 is much larger than in the standard $\Lambda \neq 0$ universe. The growth of non-linearities seems to be fastest for $n \approx 0.3$. In fact, we have already shown that the fastest growth at large a limit corresponds to the value of $n = \frac{4}{9}$. The magnitude of change in S_3 is approximately two percent with $n = 0.3$, which, although larger than in the DGP-scenario or Λ-cosmology, is out of reach of present day experiments.

However, as q is increased, also the variation of S_3 grows. For example, with $q = 10$, we see that S_3 can vary more than 10 percent from its EdS value. Also with $q \geq 2$, the values of S_3 undergo a change from values smaller than S_3^{EdS} to values larger than S_3^{EdS}. Unfortunately those changes are still unobservable.

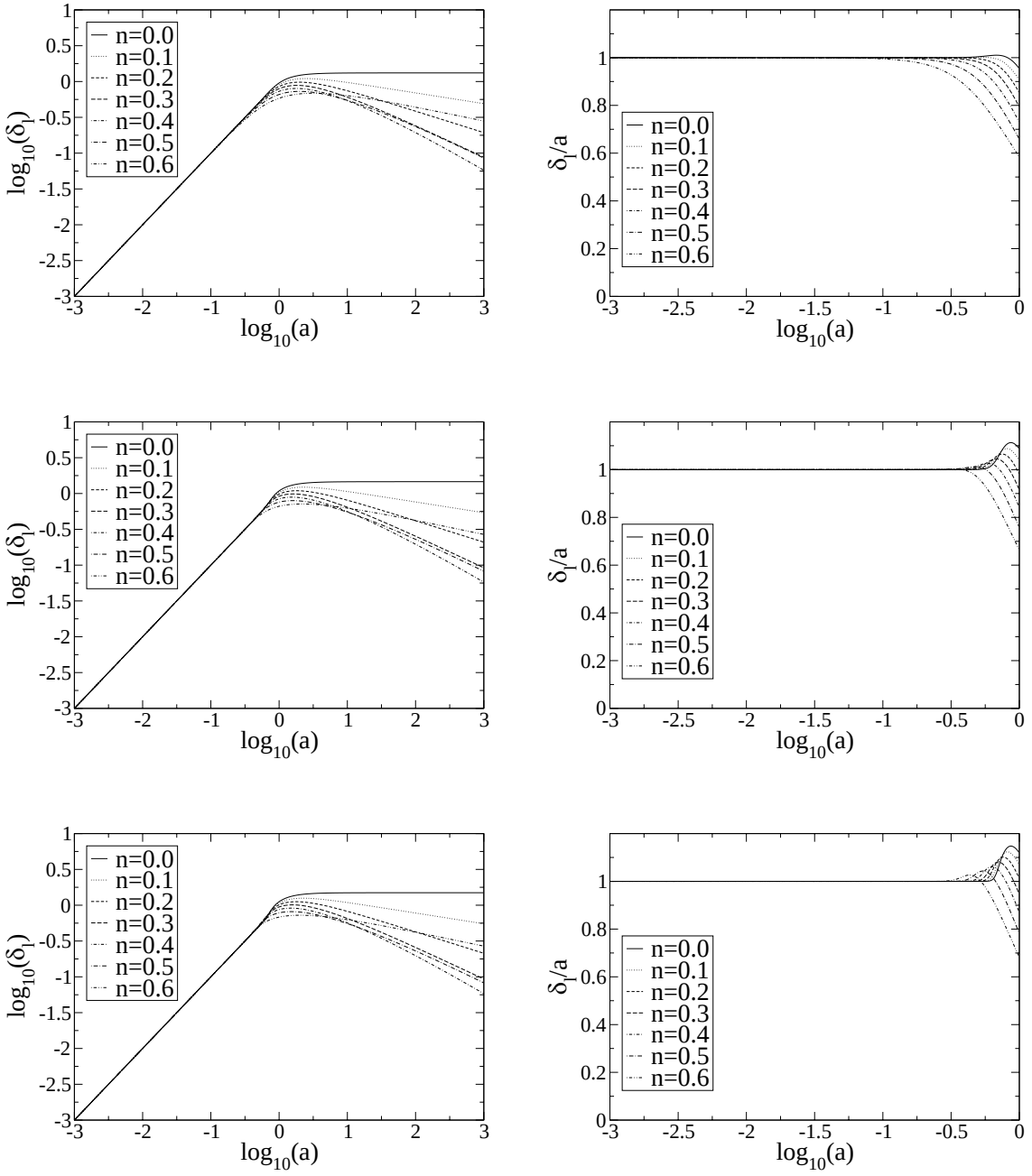

Figure 5.4: Linear growth for different values of n. Top $q = 2$, middle $q = 5$, bottom $q = 10$. In all panels $\Omega_M = 0.3$ Figures as in Multamaki, Gaztanaga & Manera (2003).

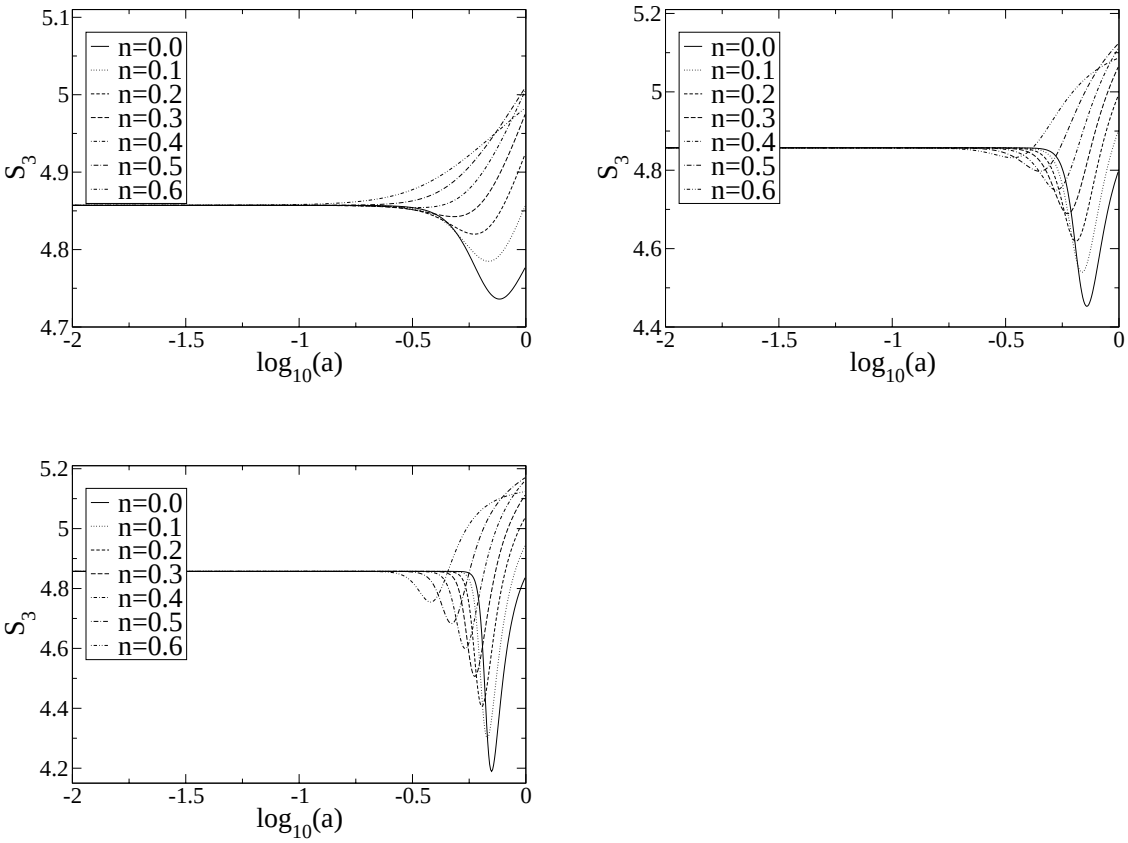

Figure 5.5: Non-linear growth (skewness) for different values of n. Top left panel $q = 2$, top right panel $q = 5$ and bottom panel $q = 10$. In all panels $\Omega_M = 0.3$ Figures as in Multamaki, Gaztanaga & Manera (2003).

Chapter 6

Non standard cosmologies III: The Chaplygin gas model

Summary

In this chapter I present the Chaplygin gas model and its linear and nonlinear growth of structure. Most results closely follow Multamaki, Manera & Gaztanaga (2004).

6.1 The Chaplygin Gas model

The General Chaplygin [1] gas, GCG, (Bento et al 2002) model introduces an non-standard perfect fluid characterized by a positive energy density and negative pressure. Its equation of state is

$$p_G = -\frac{\tilde{A}}{\rho_G^\alpha} \tag{6.1}$$

where $\tilde{A}$ is a positive (dimensionfull) constant. Such an equation of state can be the result of a scalar field with a non-standard kinetic term, *e.g.*, the string theory motivated tachyon field (Sen 2002; Gibbons 2002).

The original Chaplygin gas model (Kamenschchick et al. 2000) corresponds to the choice $\alpha = 1$. The generalization of the original Chaplygin gas to cases where $\alpha \neq 1$, was done in Bento et al.

[1] Sergei A. Chaplygin, 1869-1942

(2002) Since the original Chaplygin gas scenario is reached as a special case of the general Chaplygin gas, we will concentrate on the latter.

Using the continuity equation

$$\dot{\rho}_G + 3H(\rho_G + p_G) = 0,$$

together with the equation of state (Eq. 6.1) we can express straightforwardly the evolution of the Chaplygin density:

$$\rho_G = \rho_{G,0}\Big(A + (1-A)a^{-3(1+\alpha)}\Big)^{\frac{1}{1+\alpha}}, \tag{6.2}$$

where we have defined a useful dimensionless constant A (also often denoted as A_s in the literature), ($A \equiv \rho_{G,0}^{-(1+\alpha)}\tilde{A}$). The index 0 refers to a present day values ($z = 0$) and the new constant satisfies $0 \leq A \leq 1$ in order to have a positive energy density and negative pressure. If interested we can also express A as function of z_{sw} in which these 'two-components' of the Chaplygin gas equally contribute to the energy density.

$$A = \frac{1}{1 + (1+z_{sw})^{-3(1+\alpha)}}. \tag{6.3}$$

6.1.1 The Chaplygin gas as unified dark matter candidate

The cosmological behavior of the GCG is between a dark matter and a cosmological constant. From equations 6.2 and 6.1 we can see that at large densities, or equivalently at early times the GCG behaves as pressureless dust and $\rho_G \sim a^{-3}$, whereas at small densities, *i.e.*presently, it acts as a cosmological constant $\rho_G \approx const.$ With such a behavior one can hope to have a unified dark matter candidate, *i.e.*, one that can play both the role of cold dark matter and of the cosmological constant (Kamenschchick et al. 2000; Makler et al. 2003a). Taking a more conservative view, one can also consider a universe with both significant CDM and GCG components. Thus, the different cosmological models that include a (generalized) Chaplygin gas component can then be divided into two classes: models with and without a significant CDM component. Models that do not include a specific CDM component are often called unified dark matter (CDM) models.

Using the expressions for the energy density evolution and the Friedmann equation, one can look for solutions of $a(t)$ or $\rho(t)$. In the general case with both CDM and Chaplygin gas no analytical

solution is found. In the unified dark matter model, with only Chaplygin gas, the Friedmann equation is integrable and the solution is (up to a constant):

$$\begin{aligned} t =& \frac{2}{3}\Big(\frac{1+\frac{A}{1-A}a^{3(1+\alpha)}}{A+(1-A)a^{3(1+\alpha)}}\Big)^{\frac{1}{2(1+\alpha)}} \\ & \times \ {}_2F_1\Big(\frac{1}{2(1+\alpha)}, \frac{1}{2(1+\alpha)}, 1+\frac{1}{2(1+\alpha)}, \frac{A}{A-1}a^{3(1+\alpha)}\Big). \end{aligned} \tag{6.4}$$

In the same special case, one can also solve for the energy density (again, up to a constant):

$$t = \frac{2}{3}\frac{1}{A\kappa(1+2\alpha)}\frac{\rho^{\frac{1}{2}+\alpha}}{\rho_0^{1+\alpha}}\,{}_2F_1\Big(\frac{1+2\alpha}{2(1+\alpha)}, 1, \frac{3+4\alpha}{2(1+\alpha)}, \frac{\rho^{1+\alpha}}{A\rho_0^{1+\alpha}}\Big) \tag{6.5}$$

The unified dark matter models with a (generalized) Chaplygin gas have been studied in various works in view of cosmological observations. Cosmological perturbations of the GCG-fluid have been considered in Bento et al. (2002), Bilic et al. (2002), Fabris et al. (2002), Fabris et al. (2004), Beca et al. (2003), Bean & Dore (2003), Reis et al. (2003), Sandvik et al. (2004), Avelino et al (2004). In Sandvik et al (2004) it was claimed that the matter power spectrum strongly constrains the parameter space of unified dark matter models, essentially ruling them out. However, this result does not include the effect of the baryons and is hence questionable (Beca et al. 2003). Also, as it was pointed out in Avelino et al. (2003) and Mackler et al. (2003b), the restriction due to the matter power spectrum may be avoided by ,for instance, allowing for entropy perturbations. To complicate the matter further, in Avelino et al. (2004) it was shown that one must be careful in using linear theory to study the perturbations as linear theory may break down sooner than expected.

Other observational measures regarding the Chaplygin gas as unified dark matter include the SNIa constraints (Makler et al. 2003a; Silva & Bertolami 2003; Avelino et al. 2003), constraints coming from the CMB (Bento et al 2002; Bean & Dore 2003; Bento et al 2003a; Bento et al 2003b; Carturan & Finelli 2003) and other astrophysical data (Makler et al. 2003b; Alcaniz et al. 2003).

6.1.2 Chaplygin gas as dark energy

A significant fraction of the work in the literature has been devoted to the Chaplygin gas as an unified dark matter candidate. There is another more general approach where the Chaplygin case is considered as dark energy and therefore we also have the usual dark matter in the energy budget of

the universe. From this point of view GCG could be seen as a quintessence model with a dynamical equation of state. The Friedman equation is

$$H^2 = \frac{8\pi G}{3}(\rho_m + \rho_G), \tag{6.6}$$

Both components, the dark matter and the Chaplygin dark energy, have their own equation of state and continuity equation. Using them we can express the Friedman equation in more useful variables, the redshift and the cosmological constants $\Omega_M = 8\pi G\rho_{m,0}/3H_0^2$ and $\Omega_G = 8\pi G\rho_{G,0}/3H_0^2$. Note that we are in a flat universe and our definitions imply that $\Omega_M + \Omega_G = 1$.

Using equation 6.2 and the fact that $\rho_M \propto \rho_{M,0}\,(1+z)^3$ we can rewrite the Friedmann equation in terms of redshift as

$$H^2 = H_0^2\Big(\Omega_M(1+z)^3 + \Omega_G(A + (1-A)(1+z)^{3(1+\alpha)})^{\frac{1}{1+\alpha}}\Big), \tag{6.7}$$

We can define a redshift, z_{eq}, as the redshift where the Chaplygin gas and the dark matter equally contributes to the energy density of the universe. We can express A, and therefore the Friedmann equation, in terms of this redshift

$$A = \frac{1 - (\frac{\Omega_M}{\Omega_G})^{1+\alpha}}{1 - (1+z_{eq})^{-3(1+\alpha)}} \tag{6.8}$$

The Chaplygin gas as dark energy model reduces to a Λ CDMmodel when $\alpha = 0$ or $A = 1$. Cosmological parameters from both models can be easily related. When $\alpha = 0$ we have $\Omega_m = \Omega_M + \Omega_G(1-A)$ and $\Omega_\Lambda = \Omega_G A$, while in the case of $A = 1$ we have $\Omega_m = \Omega_M$ and $\Omega_\Lambda = \Omega_G A^{1/1+\alpha}$

As a first test for the GCG we can compare the luminosity distances in this model with the standard Λ CDM case. The luminosity distance d_L is obtained from the (line-of-sight) comoving coordinate distance: $r(z) = \int dz'/H(z')$. Using equation 2.38 we can convert luminosity distances to apparent magnitudes, and hence compare the model with SNIa data. This is what we have done in Fig. 6.1. It shows predictions for different values of A and α parameters for a fiducial $\Omega_M = 0.3$ $\Omega_G = 0.7$ GCG model. They are compared to the Λ CDMmodel and to the SNIa results (Riess et al. 1998; Perlmutter et al. 1999). It is apparent that current observations do not discriminate much between the different cosmological models. In other words: the GCG cosmologies seem to pass the

standard cosmological distance test. It is then interesting to explore whether they also pass the observational constraints on the growth of linear and non-linear structures.

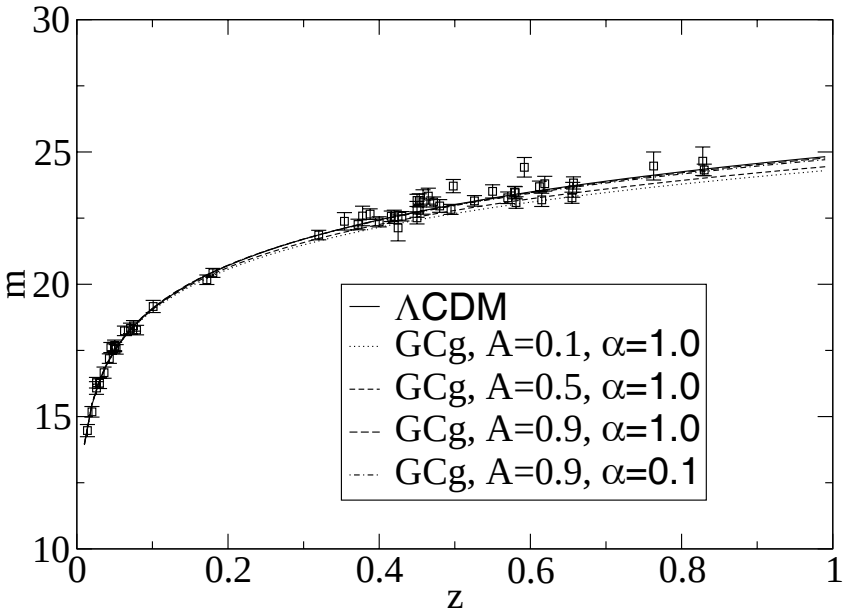

Figure 6.1: Apparent magnitudes for SNIa for different GCG cosmologies with $\Omega_M = 0.3$, $\Omega_G = 0.7$ There is a range of A and α values that could fit the data. Figure from Multamaki, Manera & Gaztanaga (2004).

The Chaplygin gas as dark energy has been studied in several works using different cosmological probes: SNIa data (Amendola et al. 2003; Bean & Dore 2003; Fabris et al. 2004; Colistete et al 2004; Cunha et al 2004), CMB fluctuations (Amendola et al. 2003; Bean & Dore 2003) or other astrophysical data like lensing (Dev et al. 2003) or globular clusters (Alcaniz et al. 2003)

Interestingly, in Fabris et al (2004) and in Colistete et al. (2004) it was found by using SNIa data that a universe dominated with a Chaplygin gas was favored over a mixed model. On the other hand, in Bean & Dore (2003) it was concluded that a Λ CDMmodel is preferred. Also in Amendola et al. (2003) using WMAP data it was shown that a CDM model is disfavored and a mixed model, with a Λ CDM-like behavior, was preferred. The bounds on the parameters are varied, depending on the type of observational data. Using globular clusters to determine the age of the universe, in

Dev et al. (2003) it was found that $\Omega_M \geq 0.2,\ A \geq 0.96$ ($\alpha = 1$), where as for the lensing statistics the bounds are somewhat looser $\Omega_M \leq 0.45,\ A_{\geq}0.72$. Using the WMAP data, in (Amendola et al. 2003) the parameter bounds were found to be $A \geq 0.8,\ 0 \leq \alpha \leq 0.2$ $(95\%CL)$ and the original Chaplygin gas was ruled out. In (Cunha et al 2004), X-rays from galaxy clusters, HST data and SNIa data were used to obtain $A \geq 0.84,\ 0.273 \leq \Omega_M \leq 0.329$ $(95\%CL)$. Using only SNIa data, it was found in (Fabris et al. 2004) for the original CG model that $A = 0.93^{+0.07}_{-0.20}$.

6.2 Growth in the Chaplygin gas model

The gravitational dynamics in the Generalized Chaplygin gas model obviously depend on the type of scenario *i.e.* whether we have a separate dark matter component or not and which components are fluctuating to form structures. Here we are considering the GCG as dark energy in the sense that it only effect the growth of the large scale structure through the background evolution. We only have perturbations in the dark matter field and we can obtain the evolution of them as in section 3.1. By using the continuity equation and the Friedmann equation we get the $\dot{H} + H^2$-term; in the GCG model it is

$$\dot{H} + H^2 = -\frac{1}{2}\frac{4\pi G}{3}\Big(\rho_M + \rho_G(1 - 3\frac{\tilde{A}}{\rho_G^{1+\alpha}})\Big) \tag{6.9}$$

We can write $\rho_M = \bar{\rho}_M(1+\delta)$, $\rho_G = \bar{\rho}_G$. Expanding according to (3.3) we find the coefficients for the differential equation.

$$\begin{aligned} c_1 &= -\frac{1}{2}\frac{\bar{\rho}_M}{\bar{\rho}_M + \bar{\rho}_G} = -\frac{1}{2}\frac{\Omega_M}{\Omega_M + \Omega_G[1 + A(a^{3(1+\alpha)} - 1)]^{\frac{1}{1+\alpha}}} && (6.10)\\ c_2 &= 0 && (6.11)\\ 2 + \frac{\dot{\bar{H}}}{\bar{H}^2} &= \frac{1}{2}(1 + 3\frac{\tilde{A}}{\bar{\rho}_G^{\alpha}(\bar{\rho}_M + \bar{\rho}_G)}) \\ &= \frac{1}{2}\Big(1 + \frac{3A\Omega_G[A + (1-A)a^{-3(1+\alpha)}]^{-\frac{\alpha}{1+\alpha}}}{\Omega_M a^{-3} + \Omega_G[A + (1-A)a^{-3(1+\alpha)}]^{\frac{1}{1+\alpha}}}\Big) && (6.12) \end{aligned}$$

6.2.1 Linear growth

Early time limit

We can take the small a limit from Eqs (6.10), *i.e.* the early time limit. The equation for the linear growth is then

$$D_1'' + \frac{1}{2} - \frac{3}{2}\frac{\Omega_M}{\Omega_M + \Omega_G(1-A)^{\frac{1}{1+\alpha}}} = 0 \tag{6.13}$$

Comparing this to the linear equation in a Λ CDM-universe,

$$D_1'' + \frac{1}{2}\frac{\Omega_M + 4a^3\Omega_\Lambda}{\Omega_M + a^3\Omega_\Lambda}D_1' - \frac{3}{2}\frac{\Omega_M}{\Omega_M + a^3\Omega_\Lambda} = 0, \tag{6.14}$$

we see that a GCG-universe behaves fundamentally differently from the Λ CDM-universe: at early times, $a \ll 1$, Λ CDM-universe reduces to the EdS-case, with solution given by Eq. (2.30), where as the GCG-universe does not. Accordingly, the solution to the linear equation in the GCG-case (in the small a limit) is

$$D_1 = B_1 e^{\frac{1}{4}(\sqrt{1+24\xi}-1)\eta} + B_2 e^{\frac{1}{4}(-\sqrt{1+24\xi}-1)\eta}, \tag{6.15}$$

where

$$\xi = \frac{\Omega_M}{\Omega_M + \Omega_G(1-A)^{\frac{1}{1+\alpha}}}. \tag{6.16}$$

Hence, EdS-case is recovered in the limits $\Omega_G = 0$ and $A = 1$. Compared to the EdS-case (and Λ CDM-universe), fluctuations therefore start to grow more slowly in a universe where GCG plays a role. Defining $\epsilon = (1-A)^{1/(1+\alpha)}\Omega_G/\Omega_M$, we see that the growing mode goes as $D_1 \sim a^{1-\frac{3}{5}\epsilon}$ when $\epsilon \ll 1$.

The large a time limit

On the other hand, in the large a limit, *i.e.*, in the far future,

$$D_1'' + \frac{1}{2}\frac{\Omega_M + 4\Omega_G A^{\frac{1}{1+\alpha}}a^3}{\Omega_M + \Omega_G A^{\frac{1}{1+\alpha}}a^3}D_1' - \frac{3}{2}\frac{\Omega_M}{\Omega_M + \Omega_G A^{\frac{1}{1+\alpha}}a^3}D_1 = 0, \tag{6.17}$$

which is the standard Λ CDM equation, Eq. (6.14), with $\Omega_\Lambda = \Omega_G A^{\frac{1}{1+\alpha}}$.

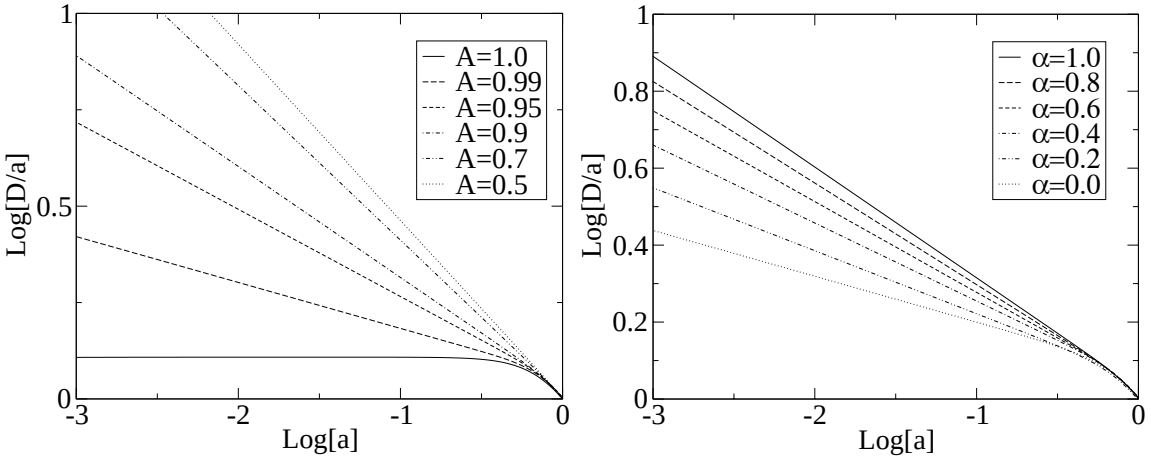

Figure 6.2: Linear growth for $\alpha = 1.0$, $A = 1, 0.95, 0.9, 0.7, 0.5$ (left panel), $A = 0.9$, $\alpha = 0, 0.2, 0.4, 0.6, 0.8, 1.0$(right panel). Figure as in Multamaki, Manera & Gaztanaga (2004).

Numerical results

In order to study the linear and non-linear evolution of the perturbation from early to late times, we must resort to numerical means. The linear and second order equations are solved numerically over the region of cosmological interest, from $a = 10^{-3}$ to $a = 1 \equiv a_0$. The initial conditions are chosen such that in both cases, the growing part of the solution, Eqs (6.15) and (6.19), is followed at early times. This ensures that the behavior of the solutions is qualitatively similar to the Λ CDM-universe and that the Λ CDM-behavior is reached as A tends to unity. Normalization is chosen so that the amplitude of fluctuations is the same at present time, *i.e.* at $a = 1$. Note that this normalization differs from the one chosen for the DGP and Cardassian models, where the amplitude of fluctuations was the same for all models at $a = 0.001$. As fiducial values we choose $\Omega_M = 0.3$, which in a flat universe sets $\Omega_G = 0.7$. We vary A and α. The case of $A = 1$ corresponds to the Λ CDM universe with $\Omega_m = 0.3$ and $\Omega_\Lambda = 0.7$.

The linear factor is plotted in Fig 6.2. Note that the linear growth is depicted relative to a, *i.e.*to the growth rate in the EdS-universe (which is also equal to the growth rate in Λ CDM-universe at early times). The linear growth rate confirms what was expected from the analytical results: linear growth occurs much more slowly than in a EdS (Λ CDM) universe until at late times when the GCG acts as a cosmological constant that dominates, leading to even stronger suppression of growth. The effect of changing α is much less significant as is shown in the left panel of figure 6.2.

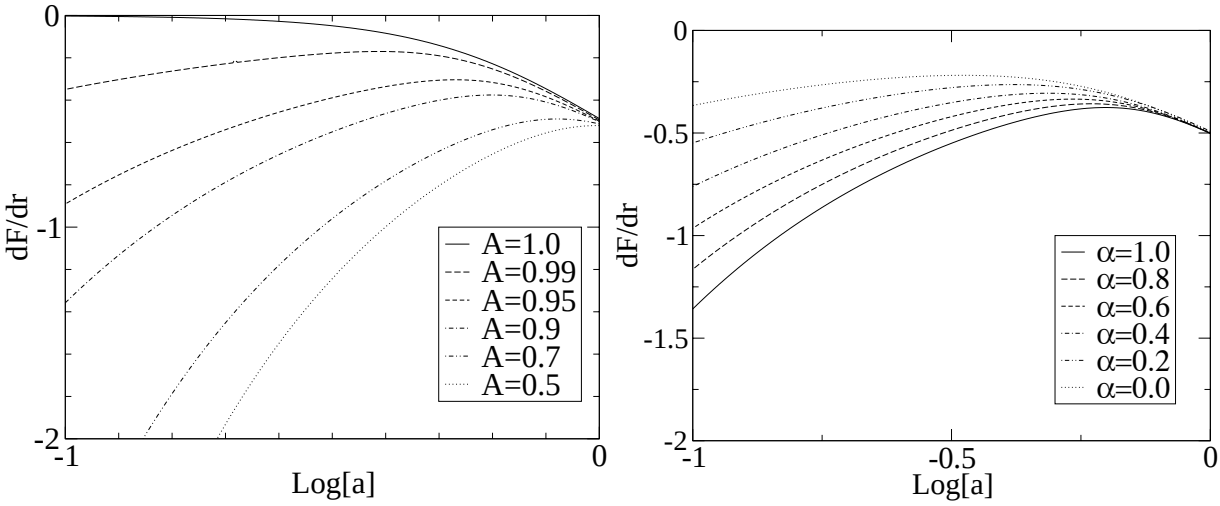

Figure 6.3: Derivative of the linear growth: $\dot{F} = d(D/a)/dr$ for $\alpha = 1.0$, $A = 1, 0.95, 0.9, 0.7, 0.5$ (left panel), $A = 0.9$, $\alpha = 0, 0.2, 0.4, 0.6, 0.8, , 1.0$(right panel). Figure as in Multamaki, Manera & Gaztanaga (2004).

We can see in Fig. 6.2 that any small deviations of the GCg parameters from the Λ CDMvalues ($\alpha = 1$ and $A = 1$) produced substantial suppression of linear growth. For example, even the case $A = 0.99$ produces a much higher amplitude of fluctuations at decoupling ($a \simeq 10^{-3}$) than the Λ CDMcosmology (when normalized at $a = 1$). Such differences in normalization are hard to reconcile with our current understanding of CMB anisotropies (see eg (Spergel et al. 2006)). The final numbers depend on the adopted model for CMB transfer function and matter content, but it is already apparent that we will need to tune the GCG parameters very close to the Λ CDMmodel. Therefore observations seem to favor values of the GCG parameters which make them equivalent to the Λ CDMcosmology.

ISW connection: linear growth evolution

As an independent test it is also interesting to study the time derivative of the above ratio: $dF/dr = d(D/a)/dr$, where dr is the comoving distance. This quantity, as it is shown in chapter 9 provides a direct observable through the Integrated Sachs-Wolfe effect (see for instance (Sachs & Wolfe 1967; Crittenden & Turok 1996; Fosalba et al. 2003). Numerical predictions for dF/dr are shown in fig. 6.3. As expected deviations from the standard Λ CDMmodel are substantial for most of the

relevant GCG parameters. In fact, again, even for $A = 0.99$ the ISW effect is much larger compared to a Λ CDM universe, thus pointing out forwards a fine tune to the parameters in order to mimic the Λ CDM cosmology. It should be stressed that in the scenario considered here, the GCG only acts through the background evolution and does not undergo gravitational collapse. Hence, these parameter constraints do not apply to the unified dark matter models with a GCG component.

Second order

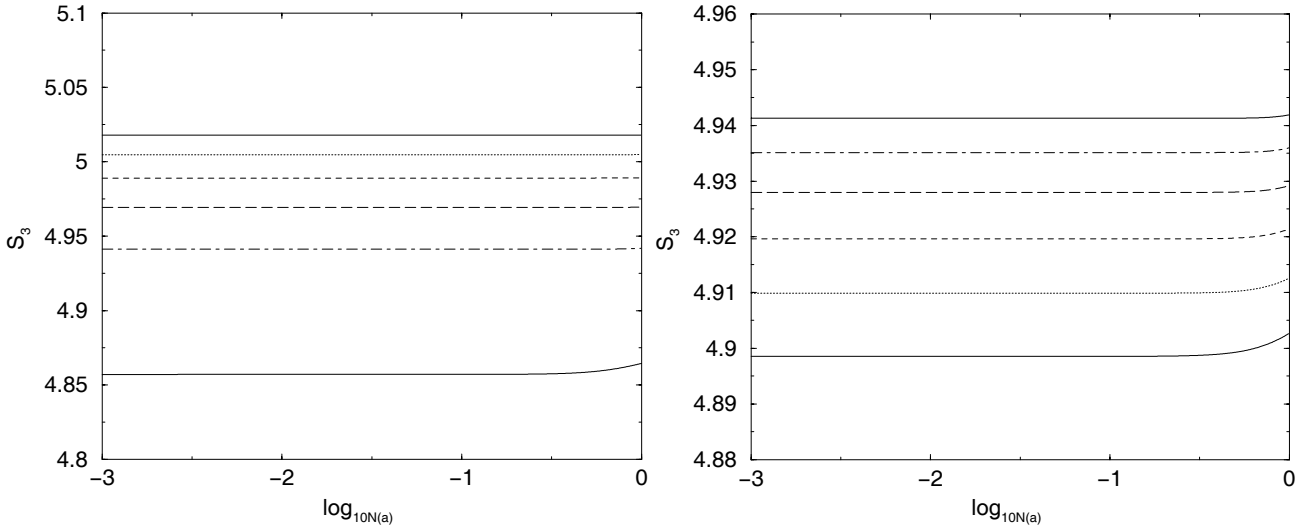

Figure 6.4: Non-linear growth for $\alpha = 1.0$, $A = 0, 0.2, 0.4, 0.6, 0.8, 1.0$ (left panel), $A = 0.9$, $\alpha = 0.2, 0.4, 0.6, 0.81.0$(right panel).

The second order equation reads at early times as

$$D_2'' + \frac{1}{2}D_2' - \frac{3}{2}\xi D_2 - \frac{8}{3}(D_1')^2 - 3\xi D_1^2 = 0. \tag{6.18}$$

Substituting the growing mode from Eq. (6.15), the solution to this equation is

$$D_2 = \frac{4}{3}\frac{\sqrt{1+24\xi}-1-21\xi}{\sqrt{1+24\xi}-1-18\xi}e^{\frac{1}{2}(\sqrt{1+24\xi}-1)\eta} + B_3 e^{\frac{1}{4}(\sqrt{1+24\xi}-1)\eta} + B_4 e^{-\frac{1}{4}(\sqrt{1+24\xi}-1)\eta}. \tag{6.19}$$

Hence, at early times, the skewness is given by

$$S_3 = 3\frac{D_2}{D_1^2} = 4\frac{\sqrt{1+24\xi}-1-21\xi}{\sqrt{1+24\xi}-1-18\xi}, \tag{6.20}$$

which when $\Omega_G = 0$ (*i.e.* $\xi = 1$) reduces to the EdS-value, $S_3^{EdS} = 34/7$. At the other extreme point, $\Omega_M = 0$ or $\xi = 0$, we reach $S_3 = 6$. All the other values lie between these two limits. When we are not in the early time limit we can solve the equation for nonlinear growth numerically. We have done so and plotted the skewness in figure 6.4. Changes from the Λ CDM cosmology are not dramatic but very small and are very well approximated by the analytical formula in eq 6.20 even for very late times. As discussed in chapter 4 such a few percent change in the skewness is not currently observable.

Chapter 7

Non standard cosmologies IV: The coupled Quintessence model

Summary

In this chapter I present the Coupled Quintessence model and its growth of structure in the spherical collapse formalism. The aim is to compute the cluster number counts and study its dependence on both the dark energy inhomogeneities and the amount of the dark matter coupled to dark energy. Most of this chapter is presented as in Manera & Mota (2006).

7.1 Motivation

Quintessence (scalar field) candidates to dark energy coupled to dark matter are strongly motivated by extra-dimensional particle physics models. A general feature of these theories, is that the size of the extra-dimensions is intimately related to a scalar field. The later is coupled to all, or a selection of matter fields (Damour et al. 1990), depending on the high energy physics model (Carroll et al. 1992; Carroll 1998; Bertolami & Mota 1999). A non-minimal coupling of the quintessence field to dark matter is therefore worth investigating (Wetterich 1995; Amendola 2000; Amendola & Tocchini-Valentini 2001; Amendola & Tocchini-Valentini 2002; Tocchini-Valentini & Amendola 2002; Mainini & Bonometo 2004; Farrar & Peebles 2004). It is then natural to think that due to this

coupling, inhomogeneities in the dark matter fluid will then propagate to the scalar field, affecting its evolution (Barrow & Mota 2003; Nunes & Mota 2006). Clearly such effect will become even more important when dark matter perturbations become non-linear. Hence, it is interesting to investigate the possibility of a dark energy component which may present inhomogeneities at cluster scales, during the non-linear regime of matter perturbations (Mota & van de Bruck 2004; Mahor & Lahav 2005).

The possible effects of dark energy inhomogeneities on cluster abundances was investigated by (Nunes et al. 2005) for minimally coupled dark energy models. Here we want to test models with dark energy coupled to dark matter using cluster number counts. So far no one has tested this until (Manera & Mota 2006) whose results I present in this chapter.

7.2 Dark Energy as a coupled quintessence field

One of the most popular candidates for dark energy is an scalar field, also known as quintessence. In the quintessence model the acceleration today would be driven by an analogous mechanism with that of the inflation, being the Lagrangian density for dark energy $\mathcal{L} = \frac{1}{2}g^{\mu\nu}\partial_\mu\phi\partial_\nu\phi - V(\phi)$. In the action principle we can derive the energy momentum tensor for the scalar field by varying the $g_{\mu\nu}$. If neglecting spatial gradients of the field we get the well known energy density and pressure expressions:

$$\begin{aligned} \rho_\phi &= \frac{1}{2}\dot{\phi}^2 + V(\phi) \\ p_\phi &= \frac{1}{2}\dot{\phi}^2 - V(\phi) \end{aligned} \tag{7.1}$$

When there is no coupling between quintessence and matter the continuity equation can be written as:

$$\ddot{\phi} + V'(\phi) + 3H\phi = 0 \tag{7.2}$$

When there is coupling between the quintessence and matter fields each component is not conserved independently. General covariance requires the conservation of the sum of the matter component $T^\mu_{\nu(m)}$ and the quintessence component $T^\mu_{\nu(\phi)}$. It is possible therefore to consider the following

coupling (Amendola 2000)

$$T^{\mu}_{\nu(\phi);\mu} = CT_{(m)}\phi_{;\mu} \tag{7.3}$$

$$T^{\mu}_{\nu(m);\mu} = -CT_{(m)}\phi_{;\mu} \tag{7.4}$$

Such a coupling arises for instance in string theory after a conformal transformation of Brans-Dicke theory (Wetterich 1995; Amendola 2000b). It is known that the quintessence coupled to dark matter system has a scaling attractor solution (Amendola 2000; Holden & Wands 2000; Tocchini-Valentini & Amendola 2002) with

$$\Omega_{\phi} = \frac{C^2 + C\alpha + 3\gamma}{(C+\alpha)^2} \qquad , \qquad \gamma_{\phi} = \frac{3\gamma^2}{C^2 + C\alpha + 3\gamma}, \tag{7.5}$$

where γ and γ_{ϕ} are the background and the scalar field equation of state respectively, and α comes from the quintessence potential $V(\phi) = V_0 \exp(\alpha\kappa\phi)$. The value of C can be extracted from Eq. (7.5). When only a fraction of dark matter is coupled (being its cosmological parameter $\Omega_{\rm cDM}$ defined as usual), a good estimate for the value of C in the tracker regime is:

$$C = -\alpha + \frac{\alpha + \sqrt{\alpha^2 - 12\tilde{\Omega}_{\rm cDM}}}{2\tilde{\Omega}_{\rm cDM}}, \tag{7.6}$$

Here $\tilde{\Omega}_{\rm cDM} = \Omega_{\rm cDM}/(\Omega_{\rm cDM} + \Omega_{\phi})$. The constraints from nucleosynthesis imply that $\Omega_{\phi}(z_{ns}) < 0.1$ (Wetterich 1995; Ferreira & Joice 1998; Sarkar 1996), which translates into $\alpha^2 > 4/\Omega_{\phi}(z_{ns})$ (Holden & Wands 2000). In the next section we will consider the growth of structure in the quintessence coupled models. There we will choose $\alpha = 10$, and C according to equation (7.6).

7.3 Growth of Structure

We consider a flat, homogeneous and isotropic background universe with scale factor $a(t)$. Since we are interested in the matter dominated epoch, we assume that the universe is filled only with cold dark matter, baryons and a quintessence field (ϕ). The Friedmann equation, which describes our

background universe scale factor, is

$$H^2 = \frac{8\pi G}{3}\left(\rho_m + \rho_\phi\right), \tag{7.7}$$

where $\rho_\phi = \frac{1}{2}\dot{\phi}^2 + V(\phi)$ and $V(\phi)$ is the scalar field potential. We assume the potential to be a pure exponential function $V(\phi) = V_0\,\exp(\alpha\kappa\phi)$, where $\kappa^2 = 8\pi G$ (in all this chapter we set $c = 1$). This is widely used in the literature. With the correct choice of the parameter α this potential leads to a late time acceleration (Amendola 2000; Barreiro et al. 2000; Copeland et al. 2004; Brookfield et al. 2006). Since we are investigating non-minimally coupled quintessence fields, ρ_m includes both the dark matter coupled to dark energy ($\rho_{\rm cDM}$) as well as the non-coupled dark matter ($\rho_{\rm um}$). We will consider different amounts of coupled matter.

The evolution of an overdensity up to the non-linear regime can be described using the spherical collapse model (see e.g. Padmanabhan 1995). The radius of the overdense region r and density contrast δ are related in this case by $1 + \delta = \rho_{\rm mc}/\rho_{\rm m} = (a/r)^3$, where $\rho_{\rm mc}$ and $\rho_{\rm m}$ are the energy densities of pressureless matter in the cluster and in the background, respectively. We consider that the cluster and the background starts differing in their evolution at $a_i = 10^{-8}$, at that time $r_i = a_i$. The energy density of cold dark matter in the background and inside the collapsing region are simply given by the following analytical solutions (see e.g. Amendola 2000)

$$\rho_{\rm um} = \rho_0\Omega_{\rm um0}\left(\frac{a_0}{a_i}\right)^3\left(\frac{a_i}{a}\right)^3, \tag{7.8}$$

$$\rho_{\rm cDM} = \rho_0\Omega_{\rm DM0}\left(\frac{a_0}{a_i}\right)^3\left(\frac{a_i}{a}\right)^3 e^{B(\phi)-B(\phi_0)}, \tag{7.9}$$

$$\rho_{{\rm um}c} = (1+\delta_i)\rho_0\Omega_{\rm um0}\left(\frac{a_0}{a_i}\right)^3\left(\frac{r_i}{r}\right)^3, \tag{7.10}$$

$$\rho_{{\rm cDM}c} = (1+\delta_i)\rho_0\Omega_{\rm cDM0}\left(\frac{a_0}{a_i}\right)^3\left(\frac{r_i}{r}\right)^3 e^{B(\phi_c)-B(\phi_0)}, \tag{7.11}$$

where again the subscripts "um" and "cDM" mean uncoupled matter and *coupled* dark matter, respectively. Uncoupled matter corresponds to both baryons and uncoupled dark matter. The

function $B(\phi)$ represents the coupling between dark energy and dark matter. We use the same coupling as in the model discussed in (Holden & Wands 2000; Amendola 2000), $B(\phi) = -C\kappa\phi$, where C is a constant. This is the coupling presented in the previous section. We choose $\alpha = 10$, and C will be chosen according to equation (7.6).

The total energy densities in the background and inside the cluster are respectively, $\rho_{\rm m} = \rho_{\rm um} + \rho_{\rm cDM}$ and $\rho_{mc} = \rho_{\rm umc} + \rho_{\rm cDMc}$ which evolve accordingly to

$$\dot{\rho}_{\rm m} = -3\frac{\dot{a}}{a}\rho_{\rm m} + \frac{dB}{d\phi}\rho_{\rm cDM}\dot{\phi}\,, \tag{7.12}$$

$$\dot{\rho}_{mc} = -3\frac{\dot{r}}{r}\rho_{mc} + \frac{dB}{d\phi_c}\rho_{\rm cDMc}\dot{\phi}_c\,. \tag{7.13}$$

The equations of motion for the evolution of the scalar field in the background and inside the overdensity are in this case (Nunes & Mota 2006):

$$\ddot{\phi} = -3\frac{\dot{a}}{a}\dot{\phi} - \frac{dV}{d\phi} - \frac{dB}{d\phi}\rho_{\rm cDM}\,, \tag{7.14}$$

$$\ddot{\phi}_c = -3\frac{\dot{r}}{r}\dot{\phi}_c - \frac{dV}{d\phi_c} - \frac{dB}{d\phi_c}\rho_{\rm cDMc} + \frac{\Gamma_\phi}{\dot{\phi}_c}\,, \tag{7.15}$$

where Γ_ϕ describes the quintessence loss of energy inside the cluster (see e.g. Mota & van de Bruck (2004) and Mahor & Lahav (2005)).

Following Mota & van de Bruck (2004) and Mahor & Lahav (2005) we study the two extreme limits for the evolution of dark energy inside the overdensity. In the first case we assume that dark energy is homogeneous, i.e. the value of ρ_ϕ inside the cluster is the same as in the background, with

$$\Gamma_\phi = -3\left(\frac{\dot{a}}{a} - \frac{\dot{r}}{r}\right)\left(\rho_{\phi_c} + p_{\phi_c}\right). \tag{7.16}$$

Hence, in this case, dark energy perturbations are not present at small scales and so $\phi_c = \phi$. In the second limit, dark energy is inhomogeneous and collapses with dark matter. Thus $\Gamma_\phi = 0$ and $\phi_c \neq \phi$. In this case perturbations in the scalar field are important at cluster scales.

In order to compute the cluster number counts we also need the evolution for the linear density

contrast (δ_L). which is given by Nunes & Mota (2006).

$$\begin{aligned}\ddot{\delta}_L &= -2H(\dot{\delta}_L - f) + \dot{f} \\ &\quad + \frac{\kappa^2}{2}\left[\rho_m\delta_L + (1+3w_{\phi_c})\delta_\phi\ \rho_\phi + 3\rho_\phi\delta w_\phi\right], \end{aligned} \tag{7.17}$$

where $\delta_\phi = \delta\rho_\phi/\rho_\phi$, with

$$\delta\rho_\phi = \dot{\phi}\,\delta\dot{\phi} + \frac{dV}{d\phi}\,\delta\phi, \tag{7.18}$$

$$\delta w_\phi = (1-w_\phi)\left(-\frac{1}{V}\,\frac{dV}{d\phi}\,\delta\phi + \delta_\phi\right), \tag{7.19}$$

and

$$f = G\left[\frac{dB}{d\phi}\,\delta\dot{\phi} + \left(\frac{dB}{d\phi}\right)^2(1-G)\dot{\phi}\,\delta\phi + \frac{d^2B}{d\phi^2}\,\dot{\phi}\,\delta\phi\right], \tag{7.20}$$

where

$$G(\phi) = \frac{\Omega_{\rm cDM0}e^{B(\phi)-B(\phi_0)}}{\Omega_{\rm cDM0}e^{B(\phi)-B(\phi_0)} + \Omega_{\rm um0}}. \tag{7.21}$$

This system of equations closes with the equation of motion for the scalar field perturbations

$$\begin{aligned}\delta\ddot{\phi} &= -3H\,\delta\dot{\phi} - \frac{dB}{d\phi}\,G\,\rho_m\delta_L + (\dot{\delta}_L - f)\dot{\phi} \\ &\quad - \left[\frac{d^2V}{d\phi^2} + \left(\frac{dB}{d\phi}\right)^2 G\,(1-G)\,\rho_m + \frac{d^2B}{d\phi^2}\,G\,\rho_m\right]\delta\phi\,. \end{aligned} \tag{7.22}$$

Integrating these equations we are now able to obtain the growth factor $D(z) = \delta_L(z)/\delta(0)$ and the linearly extrapolated density threshold above which structures will end up collapsing, i.e. $\delta_c(z) = \delta_L(z = z_{\rm col})$. Here $z_{\rm col}$ is the redshift at which the radius, r, of the overdensity is zero, and is obtained using the spherical infall model. Both of these quantities are needed to compute the number of collapsed structures following the Press-Schechter formalism (Press & Schechter 1974).

7.4 The four cases

In order to understand the cluster number counts dependence on the amount of dark matter coupled to dark energy and the behaviour of dark energy inhomogeneities during the non-linear regime, we investigate four different models/cases. We have chosen the models parameters in such a way as to have limiting cases. These give us a good understanding of the physics behind large scale structure formation and coupled quintessence models, being at the same time viable cosmological models. Below we clarify here the four cases under study. In all them we keep the fiducial values $\Omega_{m0} = 0.3, \quad \Omega_{\phi 0} = 0.7$, and $h = 0.65$.

- Model A (Homogeneous Dark Energy with a Large Amount of Dark Matter Coupled):
  All the dark matter is coupled to dark energy, $\Omega_{\rm cDM} = 0.25$. Only baryons remain uncoupled $\Omega_{\rm um} = \Omega_b = 0.05$. From equation (7.6) one has $C = 27.4$. In this model we consider that dark energy does not cluster in overdense regions. Its energy density is the same both in the cluster and in the background. Thus Γ_ϕ is the same as in equation (7.16).

- Model B (Homogeneous Dark Energy with a Small Amount of Dark Matter Coupled):
  Only a small fraction of the dark matter is coupled, $\Omega_{\rm cDM} = 0.05$. The rest is uncoupled matter $\Omega_{\rm um} + \Omega_b = 0.25$. From equation (7.6) one has $C = 139.9$. As in case A, we consider that dark energy does not cluster in overdense regions. Hence, it is a homogeneous component, with the same density all over the Universe.

- Model C (Inhomogeneous Dark Energy with a Large Amount of Dark Matter Coupled):
  All the dark matter is coupled to dark energy $\Omega_{\rm cDM} = 0.25$, only baryons remain uncoupled $\Omega_{\rm um} = \Omega_b = 0.05$. From equation (7.6), one has $C = 27.4$. In this case we consider that dark energy clusters in overdense regions. Hence, $\Gamma_\phi = 0$, which means that dark energy collapses along with dark matter.

- Model D (Inhomogeneous Dark Energy with a Small Amount of Dark Matter Coupled):
  Only a small fraction of the dark matter is coupled $\Omega_{\rm cDM} = 0.05$. The rest is uncoupled matter

$\Omega_{\rm um} + \Omega_b = 0.25$. From equation (7.6) one has $C = 139.9$. As in case C, we also consider the clustering of dark energy in overdense regions, therefore $\Gamma_\phi = 0$.

7.5 Cluster number counts dependences

In this section we compute the cluster number counts for the four models using the Press-Schechter formalism introduced in chapter 3. In order to understand the cluster number counts dependence we will look at $\bar{\rho}$,dV/dz and $\delta_c/(\sigma_8 D)$. However, we first comment on the normalization.

Normalization

We choose to normalize all models by fixing the number density of halos $n(m)$ at redshift zero. This is the normalization taken by Nunes et al. (2005). At redshift zero all models have the same comoving background density $\bar{\rho}$ and growth factor D. Therefore the only dependence on $n(m)$ is through $\delta_c(0)/\sigma_8$ (see eq 3.12). The normalization is done by adjusting σ_8 in each model such that $\delta_c(0)/\sigma_8$ is equal to the fiducial ($\sigma_8 = 0.9$) ΛCDM case. The table of computed σ_8 is presented below.

model	σ_8
ΛCDM (fiducial)	0.9
A (homogeneous, large amount coupled)	0.843
B (homogeneous, small amount coupled)	0.892
C (inhomogeneous, large amount coupled)	0.224
D (inhomogeneous, small amount coupled)	0.695

7.5.1 Dependence on the coupling between dark matter and dark energy

The coupling between dark matter and dark energy results into several signatures which distinguish these models from the minimally coupled ones. The first imprint is associated to the comoving density. In non-coupled dark energy models, as the universe evolves, the mean matter density of the universe (ρ_m), gets diluted by a^{-3} due to the expansion. In order to account for the expansion effect one constructs the comoving matter density $\bar{\rho} = \rho_m a^3$. For models with no coupling between dark matter and dark energy, $\bar{\rho}$ remains constant. However, this is not the case for coupled quintessence

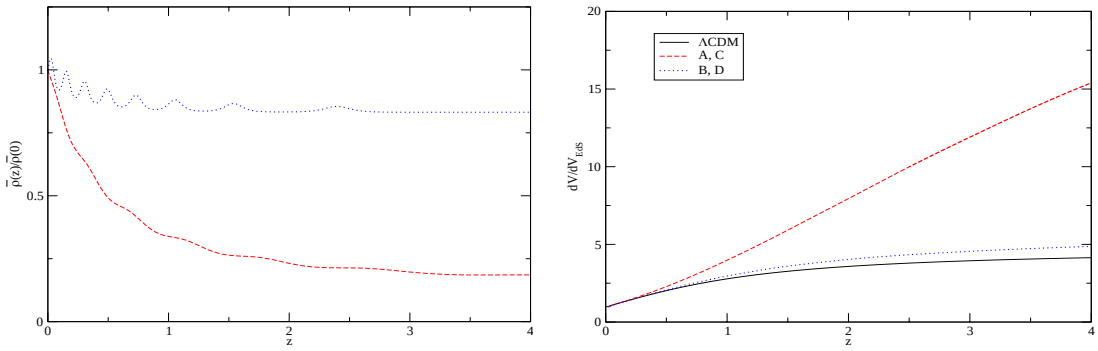

Figure 7.1: Left: Comoving background matter density as a function of redshift. There is a decrease of density because of the coupling between dark matter and dark energy. Increasing the coupling leads to a faster decreasing of the comoving density with redshift. Wiggles are a characteristic signature of coupled quintessence models. Notice that in this plot non-coupled dark energy models would correspond to a constant line equal to one. Right: Comoving volume compared to Einstein-de Sitter volume for the four study-models. Since the dark energy clustering does not affect the background evolution the difference is due only to the coupling. Models A and C with all dark matter coupled to dark energy have much more volume than models B and D, in which only a small fraction of dark matter is coupled. The concordance ΛCDM model is also plotted for comparison. Figures from Manera & Mota (2006).

models, as can be seen from equation (7.8). The wiggles that can be seen in figure 7.1 are a characteristic signature of the coupled models. They come from the oscillations in the dark energy scalar field around the minimum of the effective potential. These oscillations will be translated to the cluster number counts.

In figure 7.1 we plot the comoving matter density, in units of its present value, as a function of redshift. We can see that $\bar{\rho}$ decreases with redshift. For models with all dark matter coupled to dark energy, $\bar{\rho}$ is reduced a factor of 3 at redshift 1. Since $n(m)$ depends linearly on $\bar{\rho}$, the cluster number counts are reduced by the same factor. Notice that, in this figure, non-coupled models would have a constant line equal to one.

Coupling dark matter to dark energy not only changes $\bar{\rho}$ but also the expansion history of the universe through equation (7.7) (see e.g. (Amendola 2000) and (Tocchini-Valentini & Amendola 2002) for the evolution of background quantities). In figure 7.1 (left panel) we plot the value of dV/dz for our models A, B, C and D referenced to the Einstein-de-Sitter universe. The Concordance ΛCDM model is also plotted for comparison. Note that the volume element is a background quantity, therefore the clustering of dark energy during the non-linear regime of matter perturbations does

not affect it at all. It is clear from the figure that different possible expansions of the universe are reflected in the comoving volume element evolution with redshift. Models with more dark matter coupled to dark energy have higher values of dV/dz.

Increasing the value of dV/dz directly translates into increased cluster number counts. In fact, this effect is going in the reverse direction to the previous discussed one, i.e., increasing the volume element actually compensates or even overtakes the reduction of the number counts due to a decrease in the comoving density $\bar{\rho}$. The combination of both effects can be more clearly seen in figure 7.4, where the cluster number counts for square degree are plotted for the four models. The ΛCDM model is also plotted for comparison.

In figure 7.2 we have plotted $\delta_c(z)$ for several dark matter/dark energy couplings and for both homogeneous and inhomogeneous dark energy models. It is interesting to note the wiggles in δ_c, which are a feature of dark energy models coupled to dark matter. These wiggles come from the oscillations in the dark energy scalar field around the minimum of the effective potential. When allowing dark energy to clump with dark matter $\Gamma_\phi = 0$ (inhomogeneous models), these oscillations are strongly translated to the matter fluctuations and hence appear in δ_c. Notice that, in the homogeneous scenario oscillations are still present (see figure 5 in Nunes & Mota 2006); nevertheless they are strongly suppressed and could not be appreciated in the plot.

We plot $\delta_c/\sigma_8 D$ as a function of redshift in figure 7.3, for several case scenarios. We find that all coupled models have a ratio $\delta_c/\sigma_8 D$ below that of the ΛCDM-model. For non coupled models this is the only relevant quantity and it would have meant to expect larger halo densities than the ΛCDM model. For coupled quintessence models, however, one has also to take into account the redshift evolution of the comoving matter density, which plays a very important role as we have already seen. In fact, $\bar{\rho}$ enters both linearly and also through $\sigma(R(M, \bar{\rho}))$ in the equation for the comoving number density of collapsed objects (see Eq. (3.12)).

It is interesting to notice that both δ_c and D acquire oscillations through equation (7.17). Notice also that the typical prominent wiggles we saw in δ_c (see fig. 7.2) for inhomogeneous coupled dark energy models, cannot be seen in figure 7.3. The reason being that oscillations in δ_c are exactly compensated by oscillations in the linear growth factor when calculating the ratio $\delta_c/\sigma_8 D$.

We have plotted the redshift dependence of the cluster number counts per square degree in figure 7.4. One can see that coupled quintessence models have less number counts than the fiducial

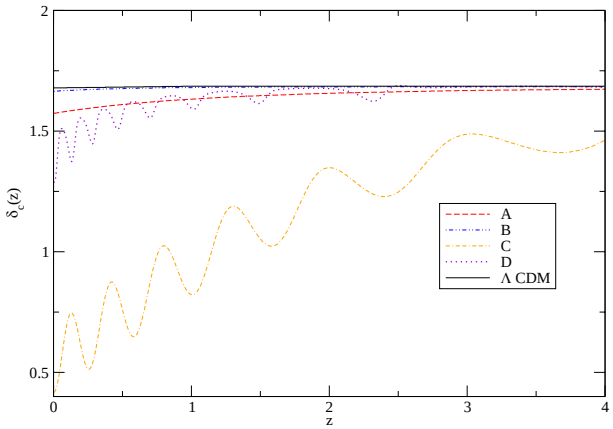

Figure 7.2: Evolution of δ_c with redshift. Model A: $\Gamma_\phi \neq 0$, $\Omega_{\rm cDM} = 0.25$, $\Omega_{\rm um} = \Omega_b = 0.05$. Model B: $\Gamma_\phi \neq 0$, $\Omega_{\rm cDM} = 0.05$, $\Omega_{\rm um} + \Omega_b = 0.25$. Model C: $\Gamma_\phi = 0$, $\Omega_{\rm cDM} = 0.25$, $\Omega_{\rm um} = \Omega_b = 0.05$. Model D: $\Gamma_\phi = 0$, $\Omega_{\rm cDM} = 0.05$, $\Omega_{\rm um} + \Omega_b = 0.25$. The ΛCDM case, solid-line, is also plotted for reference. Figure from Manera & Mota (2006)

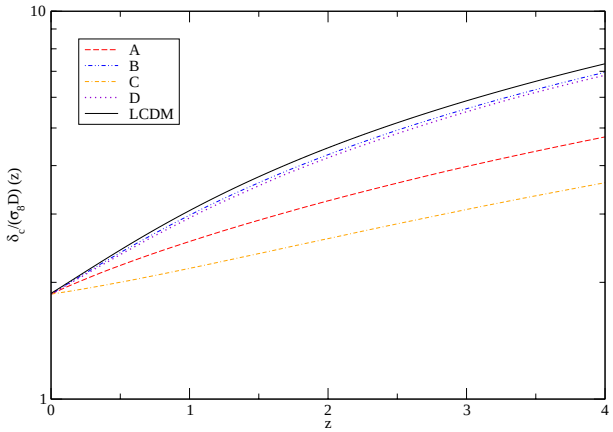

Figure 7.3: Evolution of the ratio $\delta_c/\sigma_8 D$ with redshift. Model A: $\Gamma_\phi \neq 0$, $\Omega_{\rm cDM} = 0.25$, $\Omega_{\rm um} = \Omega_b = 0.05$. Model B: $\Gamma_\phi \neq 0$, $\Omega_{\rm cDM} = 0.05$, $\Omega_{\rm um} + \Omega_b = 0.25$. Model C: $\Gamma_\phi = 0$, $\Omega_{\rm cDM} = 0.25$, $\Omega_{\rm um} = \Omega_b = 0.05$. Model D: $\Gamma_\phi = 0$, $\Omega_{\rm cDM} = 0.05$, $\Omega_{\rm um} + \Omega_b = 0.25$. The ΛCDM case is also plotted for reference. Figure from Manera & Mota (2006).

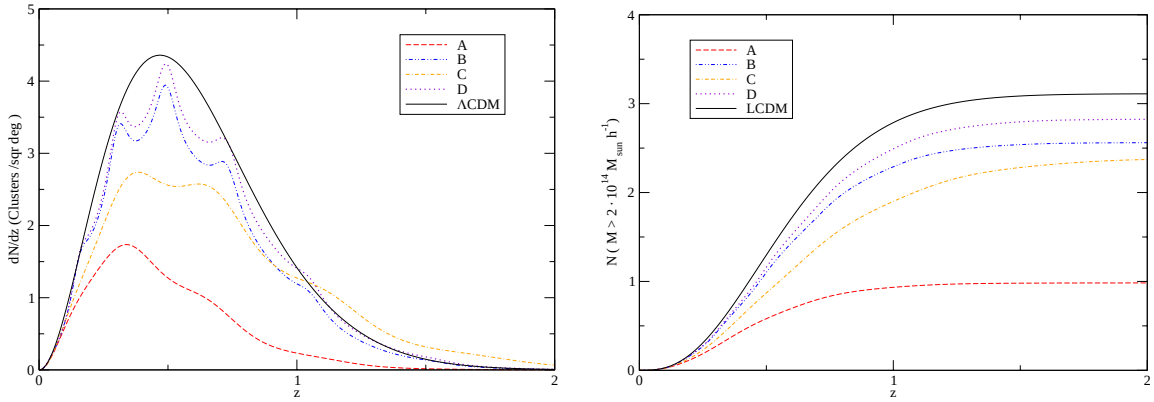

Figure 7.4: Left: Redshift dependence of the number of clusters of $M > 2.10^{14} M_{\odot} h^{-1}$ for square degree shown as in Manera & Mota (2006). Right: Integrated number of clusters of $M > 2.10^{14} M_{\odot} h^{-1}$ +up to redshift z. In both panels all models are normalized to have the same number density of halos today. ΛCDM case is also plotted for reference. Note the wiggles which are a feature of coupled dark energy models. the cluster's number counts. Note also that inhomogeneous models have more counts than their homogeneous counter-parts.

ΛCDM. Actually, increasing the amount of dark matter coupled to dark energy leads to a decrease in the number counts obtained. This is due to the different $\delta_c(z)/\sigma(M,z)$ values and the decrease of the comoving matter density, which becomes more important than the larger accessible volume.

We have also plot, in figure 7.4 (left panel), the integrated number of dark matter halos with $M > 2.10^{14} M_{\odot} h^{-1}$ up to redshift z per square degree. Once again, all models are normalized to have the same number density of halos today. The ΛCDM case is also plotted for reference. In concordance to what we saw for the cluster abundances, increasing the amount of dark matter coupled to dark energy leads to a decrease of the integrated cluster number counts. The differences between integrated counts results from the same combination of effects just discussed previously. In our work we have obviously not performed the integration in the mass range all the way up to infinity, but to $M_{\rm sup} = 10^{16} h^{-1} M_{\odot}$. This is enough due to the exponential cutoff for the cluster number counts in mass (see Eq. (3.12)). The difference between the integrated number counts of a model with respect to the cosmological constant model becomes constant above a certain redshift $z_{\rm flat}$. This is so because the number counts (Eq. (3.9)) decrease exponentially with redshift. Hence contributions above $z_{\rm flat}$ become negligible. For the models studied here this regime starts at $z_{\rm flat} \simeq 2$.

A peculiarity of models where dark energy is coupled to dark matter are the oscillations present

at the cluster number counts (see fig. 7.4). Wiggles are in fact a common characteristic of coupled quintessence models. These appear when the scalar field oscillates about the minimum of its effective potential. Due to the coupling to dark matter, these oscillations are transfered to the dark matter fluid, and induce a corresponding oscillation in the $\rho_{\rm cDM}$ and $\rho_{\rm cDM}c$ components (see Fig. 7 of Copeland 2004). Notice, however, that these wiggles are related to the quintessence potential form and initial conditions for the scalar field (Mota & van de Bruck 2004; Nunes & Mota 2006). For instance, other coupled quintessence models which would have an effective potential without a minimum may not present such wiggles. Similarly, a different choice of initial conditions for the scalar field may lead to the case where the field did not have time to reach the minimum of its potential today. Hence, one would not see the oscillations. Nevertheless, fluctuations in the cluster number counts if detected would likely indicate the existence of a coupling between dark energy and dark matter.

7.5.2 Dependence on the dark energy inhomogeneities

From figure 7.4, it is clear that models with clustering dark energy (inhomogeneous models) have more number counts than their homogeneous counterparts. This can be understood looking at δ_c and the ratio $\delta_c(z)/\sigma_8 D(z)$ (see figures 7.2 and 7.3). When dark energy clusters with matter, it acts as a negative pressure slowing the growth of structures. Models with a linear growth factor increasing slowly have more structure in the past because we normalize all cases such that we have the same number density of halos today. In fact, the density of collapsed objects is very sensitive to the linear growth factor and to the critical density $\delta_c(z)$. For inhomogeneous dark energy models, it turns out to be significantly lower than the fiducial ΛCDM model (see figure 7.2). This is also the reason for their low σ_8 in the normalization table.

Wiggles are a common feature for both the homogeneous and inhomogeneous cases. There are, however, some differences between these cases. In the homogeneous models wiggles are basically only prominent in background quantities, i.e, $\bar{\rho}_m$ (see fig. 7.1), while remain very supressed in clustered related quantities like δ_c and the linear growth factor δ_L (see figure 7.2). In contrast, in the inhomogeneous cases, due to the clustering of dark energy, wiggles will also quite distinctly appear in δ_L and δ_c (see again figure 7.2). Independently of the clustering properties of dark energy, oscillations in cluster number counts will appear, in coupled quintessence models, due to oscillations

in the background density. These oscillations are propagated via the Press-Schechter formalism to the cluster number counts.

7.6 Discriminating models with future surveys

It is important to estimate whether future surveys measuring cluster abundances will be able to discriminate among different dark energy models. In order to assess such possibility we test our dark energy model B: Homogeneous dark energy component with a small amount of dark matter coupled. The aim here is not to perform a detailed analysis but to get an idea of the potential detectability of the features of coupled quintessence models.

Bahcall & Bode (2003) have used the abundance of massive clusters ($m > 8 \cdot 10^{14} M_{\odot}$) in the redshift range $z = 0.5 - 0.8$ to constrain the amplitude of fluctuations σ_8 within 10% in the ΛCDM case. Such uncertainty in σ_8 comes from the presence of very large errors in cluster number counts, which are big enough for different models to survive. Moreover, errors in the mass determination of clusters also significantly change the expected number counts (Lima & Hu 2005).

In the near future new surveys are planned to specifically find clusters in the sky. The South Pole Telescope (SPT) (Ruhl J et al. 2005 (SPT Collaboration)), which is currently under construction, will use the Sunayev-Zeldovich effect to find clusters and determine their masses. Also the recently proposed Dark Energy Survey (DES) ((Annis J. et al.))[1] will observe almost the same region of the sky and provide redshifts for those clusters. Both surveys will share an area of 4000 square degrees in which two thousand clusters are expected to be found. Such large numbers will allow to better test and discriminate dark energy models. The expected errors in redshift for the SPT+DES clusters are $\sigma_z = 0.02$ for clusters with $z < 1.3$ and $\sigma_z < 0.1$ for clusters in the redshift range $1.3 < z < 2$. Where σ_z encompasses the 68% probability for the redshift being in the $z \pm \sigma_z$ range.

In order to explore the potential detectability of wiggles in the cluster number counts from these future surveys, we fit model B with a flat ΛCDM model by varying σ_8 and Ω_m. We simply integrate the cluster number counts for all 4000 deg DES+SPT survey in redhift bins. We choose to use bins of width 0.05 for $z < 1.3$ and 0.1 within the range $1.3 < z < 2$, to be consistent with the expected

[1] Dark Energy Survey: http://cosmology.astro.uiuc.edu/DES/ http://www.darkenergysurvey.org

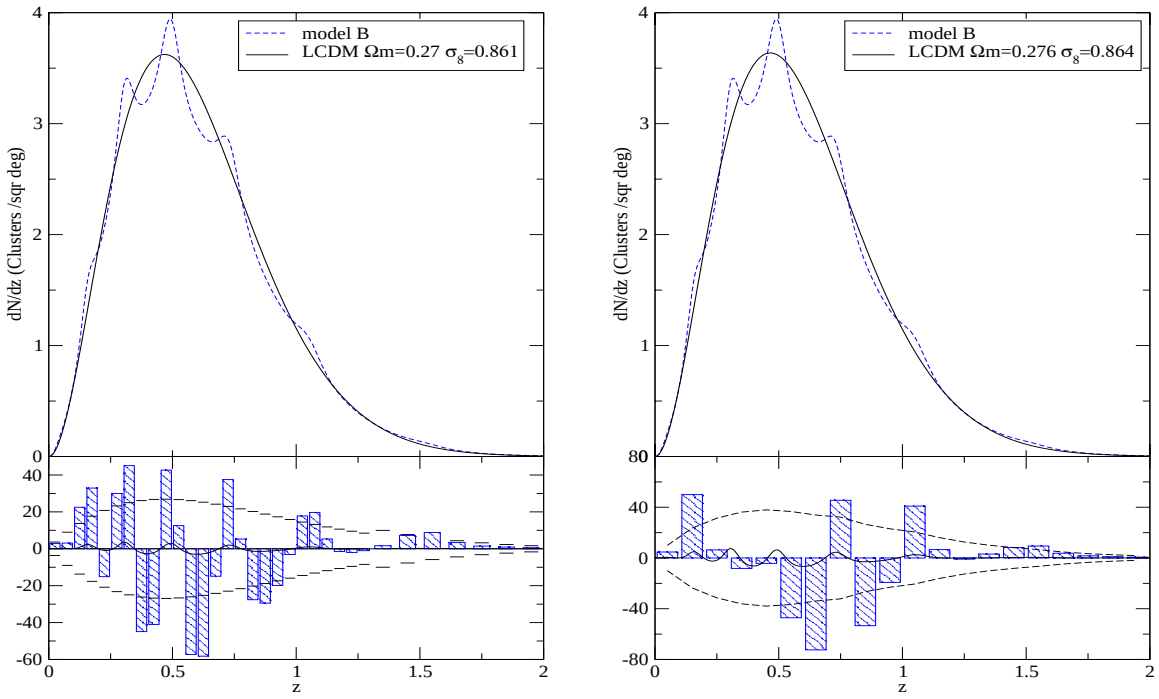

Figure 7.5: Top left panel: Cluster number counts for model B (dashed line) along with a ΛCDM fit for the model (solid line). The fit is done by adjusting σ_8 and Ω_m. Bottom left panel: Cluster number counts for the 4000deg DES+SPT survey in redshift bins of 0.05. Horizontal bars show shot-noise errors for the bins. Solid line shows the wiggles as a difference between model B and the fit in an arbitrary scale. Right: Same as left panel with slightly different good fit and bins of 0.1 in redshift.

observational errors. The best fit is obtained by minimizing χ^2

$$\chi^2 = \sum_{bins} \frac{\left(N_i^{modelB} - N_i^{\Lambda CDM}(\Omega_m, \sigma_8)\right)^2}{\sigma_{SN}^2} \tag{7.23}$$

where N_i is the number of clusters in the ith bin and σ_i^{SN} is its shot noise error, which is the expected error in any counting statistics. The best fit corresponds to $\Omega_m = 0.27$ and $\sigma_8 = 0.861$. Both the best fit and model B are shown in the top left panel of figure 7.5. In the bottom panel we plot the difference of the binned cluster counts between the model and the fit. This difference is also in redshift bins. In the bottom panel we also plot in horizontal bars the shot noise error for each bin. The continuous line represents the unbinned difference between model B and the fit. For clarity, this difference is arbitrarily scaled. It is plotted only to see the correspondence between bins, wiggles and the smoothing due to the binning. We notice that the best fit is almost degenerate with slightly different cosmological parameters. In figure 7.5 (right panel) we plot the model B for with $\Omega_m = 0.276$ and $\sigma_8 = 0.64$. We show bins of 0.1 in redshift for this case. Since these bigger bins we will produce a lower signal to noise we focus on discussing the detection of the smaller bin case.

In this section we are interested in having a broad idea about the potential detection of the cluster number counts oscillations, which are a special feature of coupled quintessence models. To answer this, one could ask how significant is the difference between the model and the fit, given the expected errors for the cluster number counts in each redshift bin. The minimum χ^2 for this realization is 47.7, which gives a probability of less than 5% for the wiggles being explained by stochastic fluctuations from the best fit ΛCDM model. We also performed a Kolmogorov-Smirnov test, which is less sensitive to the tidal parts of the distribution. After smoothing the wiggles signature with a Gaussian beam of half-width= 0.05 in redshift to simulate the errors, the Kolmogorov-Smirnov test gives a probability $\sim 6\%$ for ΛCDM being the underlying model. Hence, both the χ^2 test as well as the Kolmogorov-Smirnov test seem to indicate that future surveys could possibly detect those oscillations in the cluster abundances.

Chapter 8

Discriminating non-standard cosmological models

Summary

In this chapter I summarize the results of the Part I of this thesis, focusing on relating non-standard evolution of structures with observations.

8.1 Conclusions

In the Part I of this thesis we studied four non-standard models: the Dvali Gabadadze and Porrati model (DGP), the Original and Modified Polytropic Cardassian model (MPC), the Generalized Chaplygin Gas model (CG), and the Coupled Quintessence model. The growth of structure in the first three non-standard models was studied using a formalism introduced in chapter 3. The aim of the formalism is to get a useful approximation for the growth of the matter perturbations for those modified gravity theories that provide a Friedmann equation. Instead of solving the full perturbation theory of the modified gravity cosmology we will use the Raychaudhuri's equation together with the Friedmann and continuity equation to get the evolution of spherical perturbations. This would give the exact linear growth and the correct leading order non-linear perturbations for spherical windows as well as the Press-Schechter number counts.

The growth of large scale structure is, in fact, tightly bound to the overall evolution of the universe and hence to the particular cosmological model. As such, along with the SNIa and CMB data, it is a powerful tool to probe the space of possible cosmologies. In order to evaluate the significance of the non-standard evolution of large scale perturbations, one obviously needs to relate the predictions of the linear and the non-linear growth to observations. We have done this mainly by looking at σ_8, the skewness S_3 and the cluster number counts. Below I summarize the results:

Linear growth

Like in the standard Λ CDM cosmology, in the studied non-standard models it was found that linear growth is generally inhibited due to the accelerated expansion. In the DGP and the Cardassian models, depending on the values of the parameters, the suppression at present compared to the EdS-case can be as much as 50%. In the Modified Polytropic Cardassian model, however, there is an exception in which, for certain parameter values and a limited range of redhift, the linear growth can actually be faster than in the EdS universe. This is an interesting property since models that have late time acceleration typically lead to less linear growth at all times.

The linear normalization of large scale density fields vary greatly within models. When normalizing the models at hight redshift the value of σ_8 can be much smaller in the MPC- and DGP-scenarios than the value in the standard Λ-cosmology. Also the quintessence models, when normalized to have the same amount of clusters today, present a lower σ_8 than the concordance Λ CDM cosmology. Intriguingly, there is already some observational indication of a small value of σ_8 at low red-shifts (clusters abundances tend to give lower values than CMB studies) but more observational data is needed in order to determine whether this effect is real. In any case, observations of σ_8 at low red-shifts, combined with the precision CMB data from the *WMAP* (and in the future *Planck*) mission, is becoming a powerful probe of non-standard cosmological evolution.

The linear growth of structures in the Generalized Chaplygin gas scenario is very sensitive to the value of the parameters. In fact, any small deviation from the parameters that recover the Λ CDM cosmology produces a substantial suppression of the linear growth. Thus this model where Chaplygin gas acts only as dark energy, i.e. it doesn't undergo gravitational collapse, turns out to be very hard to reconcile with CMB anisotropies. The ISW effect would be also much larger in the Chaplygin model than in the Λ CDM cosmology even for $A = 0.99$. Therefore, we conclude that the

Generalized Chaplygin gas as dark energy does not seem to provide any apparent advantage over the simpler Λ CDM model. However, other approaches to Chaplygin gas, as for instance the two fluid interpretation, might do so. Thus they are also worth investigating.

Non-linear growth

The non-linear growth for DGP and Cardassian models was studied by considering the value of the skewness, S_3, whose evolution can be straightforwardly extracted in each model. Deviations from the EdS-value are only of order of one percent in the DGP scenario and can vary up to 10% for the MPC model. Unfortunately observations does not determine yet the skewness with such precision.

Another quantity that is strongly affected by the non-standard linear evolution is the number counts of objects. The Press-Schechter formalism gives strong predictions for the number of clusters that differ significantly from what one expects in a Λ-cosmology. The DGP and the MPC models predict two and four times more clusters at $z \simeq 1.5$ than the Λ CDM cosmology.

For the coupled quintessence models we have shown that there is a significant dependence of cluster number counts on dark energy inhomogeneities and on the amount of dark matter coupled to dark energy. Increasing the coupling between dark matter to dark energy reduces the cluster number counts. This effect is due to the decrease of the comoving matter density and the distinctive evolution of δ_c/σ in time. Dark energy clustering is shown to increase cluster number counts by slowing down the formation of structure. Hence, depending on the amount of coupling between dark energy and dark matter and on the clustering properties of dark energy, these effects can combine together or against each other to strongly increase or reduce cluster abundances.

Oscillations in cluster number counts in redshift, are found to be a specific signature of quintessence models with dark matter coupled to dark energy. In homogeneous dark energy models, these oscillations are mainly present in background quantities, such as $\bar{\rho}_m$, while in the inhomogeneous case the oscillations also appear in perturbed quantities, like δ_c. We have shown that such fluctuations are propagated to the cluster number counts producing this very peculiar cosmological imprint.

We investigated the possibility of near future observations to discriminate between quintessence models coupled to dark matter and the Λ CDM cosmology. We tested the particular quintessence model of where dark energy is coupled to a small amount of dark matter and where dark energy is homogeneous at cluster scales. We fit this model to a flat ΛCDM-model by varying σ_8 and Ω_m and

minimizing the χ^2. We find that a future DES+SPT like survey could likely be used to differentiate it from the Λ CDM, thus showing the potential that studying the number counts of clusters at different redshifts has in order to constrain non-standard cosmological models.